

Impact of grain evolution on the chemical structure of protoplanetary disks

A.I. Vasyunin

Max Planck Institute for Astronomy, Königstuhl 17, D-69117 Heidelberg, Germany

*Department of Physics, The Ohio State University, 191 W. Woodruff Ave., Columbus OH,
43210, USA¹*

vasyunin@mps.ohio-state.edu

D.S. Wiebe

*Institute of Astronomy of the Russian Academy of Sciences, Pyatnitskaya str. 48, 119017
Moscow, Russia*

dwiebe@inasan.ru

T. Birnstiel

Max Planck Institute for Astronomy, Königstuhl 17, D-69117 Heidelberg, Germany

birnstiel@mpia.de

S. Zhukovska

Max Planck Institute for Astronomy, Königstuhl 17, D-69117 Heidelberg, Germany

zhukovska@mpia.de

T. Henning

Max Planck Institute for Astronomy, Königstuhl 17, D-69117 Heidelberg, Germany

henning@mpia.de

C.P. Dullemond

Max Planck Institute for Astronomy, Königstuhl 17, D-69117 Heidelberg, Germany

dullemon@mpia.de

ABSTRACT

We study the impact of dust evolution in a protoplanetary disk around a T Tauri star on the disk chemical composition. For the first time we utilize a comprehensive model of dust evolution which includes growth, fragmentation and sedimentation. Specific attention is paid to the influence of grain evolution on the penetration of the UV field in the disk. A chemical model that includes a comprehensive set of gas phase and grain surface chemical reactions is used to simulate the chemical structure of the disk.

The main effect of the grain evolution on the disk chemical composition comes from sedimentation, and, to a lesser degree, from the reduction of the total grain surface area. The net effect of grain growth is suppressed by the fragmentation process which maintains a population of small grains, dominating the total grain surface area. We consider three models of dust properties. In model GS both growth and sedimentation are taken into account. In models A5 and A4 all grains are assumed to have the same size (10^{-5} cm and 10^{-4} cm, respectively) with constant gas-to-dust mass ratio of 100. Like in previous studies, the “three-layer” pattern (cold midplane, warm molecular layer, and hot atmosphere) in the disk chemical structure is preserved in all models, but shifted closer to the midplane in models with increased grain size (GS and A4). Unlike other similar studies, we find that in models GS and A4 column densities of most gas-phase species are enhanced by 1–3 orders of magnitude relative to those in a model with pristine dust (A5), while column densities of their surface counterparts are decreased. We show that column densities of certain species, like C_2H , $HC_{2n+1}N$ ($n = 0 - 3$), H_2O and some other molecules, as well as the C_2H_2/HCN abundance ratio, which are accessible with Herschel and ALMA, can be used as observational tracers of early stages of the grain evolution process in protoplanetary disks.

Subject headings: accretion disks, astrochemistry, opacity, ultraviolet: planetary systems

1. Introduction

The presence of numerous exoplanets and protoplanetary disks (PPD), as well as our own existence, strongly suggest that planet formation is ubiquitous in the Milky Way (e.g., Mayor & Queloz 1995; Mayor & Frei 2003; Udry & Santos 2007). Still, it is one of the most

¹Moved in September 2010

challenging problems for the modern astronomy to understand how planets form. This topic covers a tremendous range of micro- and macrophysics, and involves a wide variety of physical, dynamical, and chemical processes.

According to the current paradigm, planets are assembled in protoplanetary disks surrounding young stars, starting from the coagulation of sub-micron dust grains into larger bodies (e.g., Natta et al. 2007; Henning 2008). Circumstantial evidence indicates that this process is quite effective and rapid. For example, large-scale IR spectroscopic surveys of young stars in stellar clusters of various ages tightly constrain typical dispersal timescales of circumstellar dust disks of $\sim 5 - 10$ Myr, and mass accretion rates of $\dot{M}_{\text{Sun}} \sim 10^{-8} M_{\odot} \text{ yr}^{-1}$ (Haisch et al. 2001; Sicilia-Aguilar et al. 2006; Hernández et al. 2008; Oliveira et al. 2009; Sicilia-Aguilar et al. 2009; Fedele et al. 2010). Inner, planet-forming zones of some older disks are cleared of sub-micron-sized dust grains within just ~ 1 Myr (e.g., Graham et al. 2007; Dutrey et al. 2008; Salyk et al. 2009; Thalmann et al. 2010). Furthermore, the analysis of the mineralogical and chemical composition of unaltered chondritic meteorites shows that in the Solar Nebula different types of meteorites have condensed and formed via grain agglomeration within a period of $\sim 2 - 5$ Myr (e.g., Wasson & Kallemeyn 1988; Podosek & Cassen 1994; Thrane et al. 2006).

However, observational data on grain growth are still scarce and limited to the overall spectral energy distribution (SED) parameters. The presence of micron-sized grains in disks has been inferred from mid-infrared spectroscopy (e.g., Bouwman et al. 2001, 2008; Apai et al. 2004; van Boekel et al. 2004; Kessler-Silacci et al. 2006). A number of nearby protoplanetary disks has been imaged with the VLA and Australia Telescope Compact Array (ATCA) at millimeter and centimeter wavelengths, showing evidence of significant grain growth up to at least pebble (cm) sizes (Testi et al. 2003; Wilner et al. 2005; Rodmann et al. 2006; Natta et al. 2007; Cortes et al. 2009; Lommen et al. 2009). On the other hand, there can be other observables indicative of the grain ensemble evolution.

In essence, grain evolution is controlled by collisions, leading to coagulation and fragmentation of dust particles. For mm-sized particles the bouncing effect comes into play, making the process more complicated and further growth less efficient (Zsom et al. 2010). Radial drift and sedimentation to the disk midplane become important if the growth of grain particles proceeds further than about 1 cm. Grains evolve faster in the dense disk interior ($\lesssim 10 - 20$ AU), while in the outer regions ($R \gtrsim 100$ AU), the grain ensemble may remain unchanged (ISM-like) for the entire life of the system (Schmitt et al. 1997; Weidenschilling 1997; Ciesla 2007; Ormel et al. 2007; Brauer et al. 2008a; Birnstiel et al. 2009, 2010). It is therefore reasonable to expect that the evolution of grain sizes and spatial distribution is somehow reflected in the physical and chemical structure of the disk.

In current models of disk structure it is assumed that the temperature distribution within the disk, and thus its structure, is controlled by the radiative transfer of energy generated due to viscous dissipation and absorption of the stellar radiation. In the disk atmosphere, photoelectric heating from dust grains becomes important for energy balance (e.g., Gorti & Hollenbach 2009; Woitke et al. 2009). Dust opacities, which are changed by grain growth and sedimentation, are the crucial element in this picture. Also, because of dust evolution, stellar UV photons penetrate more easily into the disk interior, heating it, and thus preventing rapid freeze-out of molecules and enhancing photodestruction of gas-phase chemical species (e.g., Aikawa & Nomura 2006; Jonkheid et al. 2006, 2007). Local variations in the dust-to-gas ratio, dust density and average grain size may all affect the efficiency of gas-grain interactions, and thus the efficiency of freeze-out and surface chemistry.

The problem of possible interrelations between dust evolution and chemistry has been addressed in the literature a number of times. Jonkheid et al. (2004) studied the importance of dust settling on the disk chemical evolution, assuming that the dust size distribution remains the same along the disk radius. It was found that dust sedimentation has a great impact on the gas temperature in the disk and that dust and gas temperatures are significantly different in the optically-thin disk region. On the other hand, sedimentation was found to not strongly influence the gas-phase chemistry in the model considered due to the assumption that PAHs are still well-mixed with the gas and therefore efficiently absorb stellar and interstellar UV photons. At the same time, elevated temperatures of the upper disk layer in the model with grain sedimentation lead to excitation of higher-lying transitions.

Aikawa & Nomura (2006) considered the effect of dust growth on chemical abundances in a well-mixed disk around a low-mass star. They modeled dust and gas temperatures in the disk self-consistently and adopted a power-law grain size distribution. The grain growth was simulated by raising the maximum grain size up to $10\mu\text{m}$. An extended chemical network with gas-grain interactions and surface processes was applied. They found that the main effect of dust growth is a shift of the molecular layer towards the disk midplane. At the same time, column densities for many species were not affected by grain growth. Finally, they identified a few sensitive tracers of grain growth in disks, such as HCO^+ , H_3^+ , H_2D^+ .

Later, Jonkheid et al. (2007) modeled chemistry and gas temperature of evolving Herbig Ae disks with decreasing mass or dust settling. They utilized a 2D radiative transfer code to model gas/dust temperature and photodissociation rates. It was found that the disk chemical structure strongly correlates with the disk mass: while some photofragile molecules like HCN are abundant only in massive disks, their fragments, like CN and CCH, become abundant in low-mass disks. Furthermore, dust settling affects the gas temperature in the disk atmosphere, and consequently abundances of disk atmosphere tracers like O and C^+ .

They identified that line intensity ratios of CO/ ^{13}CO , CO/HCO $^+$ and [OI] 63 μm /146 μm can be used to distinguish between disks undergoing grain settling and photoevaporated disks.

In the present work, we move one step further and omit the simplifying assumptions that grain evolution proceeds uniformly over the entire disk, or that it can be described by artificially varying the grain number density and upper grain size limit. The goal is to isolate possible molecular tracers of grain evolution in the situation when grain size distribution and dust-to-gas mass ratio vary smoothly in the disk, as predicted by a dust evolution model. The model used includes coagulation, fragmentation, and sedimentation, assuming equilibrium between turbulent stirring and gravitational settling, as proposed in Dullemond & Dominik (2004). No bouncing effects are included. We focus on the combined effect of dust growth and settling on the chemistry in a protoplanetary disk around a low mass T Tauri star. A large gas-grain chemical network with surface reactions is utilized. This is the first paper in a series, where we intend to study various aspects of interrelations between grain evolution and chemistry.

The outline of the paper is the following. In section 2, the setup we constructed to model the physical structure of disk with evolving dust is described. Section 3 contains a description of the detailed chemical model used to simulate the chemical structure of the protoplanetary disk. In section 4 we present modeling results. In paragraph 4.1 dust evolution due to growth, fragmentation and sedimentation is discussed briefly. In paragraph 4.2 change to the UV field in the disk caused by evolution of dust properties are discussed. Paragraph 4.3 is devoted to the analysis of the impact of grain evolution on the chemistry of a protoplanetary disk. In section 4, we discuss whether or not the chemical composition of a protoplanetary disk can be used as a tracer of grain evolution, and in which ways our model can be improved. Section 6 contains the conclusions of this study.

2. Description of the model

A protoplanetary disk, even in a simplified description is a complicated evolving system controlled by a large number of interrelated physical and chemical processes. However, given the uncertainties and deficiencies in the physical description of such a system, it would be impossible and impractical to try to build a self-consistent dynamical model coupled to grain evolution and disk chemistry. For this reason, we have selected an approach which is by no means self-consistent, but is relatively straightforward to implement and allows us to isolate the purely chemical effect of the dust growth.

The disk chemical modeling in this study comprises of four independent steps. First, we

need a template of a disk physical structure, i.e. gas density and temperature distributions. These distributions are obtained from a 1+1D steady-state accretion disk model. In the second step, the resulting thermal and density structure is used as an input for the grain growth model. The third step is to simulate the evolution of the dust grain ensemble in the disk midplane due to grain coagulation, fragmentation and sedimentation according to Birnstiel et al. (2009, 2010). Third, the vertical distribution of dust is reconstructed in stirring-mixing equilibrium based on the work by Dullemond & Dominik (2004).

Finally, the grain parameters (size distribution at each disk location, as well as dust-to-gas ratios) after 2 Myr of evolution are used in the simulation of the disk chemical structure. These steps are described in more details in the following subsections.

2.1. Physical structure of the disk

A popular formalism, which is used in many studies of disks surrounding young stars, is based on the so-called α -model of Shakura & Sunyaev (1973). In this model it is assumed that the transport of angular momentum in the disk is caused by turbulent viscosity, with the viscosity coefficient ν expressed as $\alpha H c_s$, where H is the disk semi-thickness at a given radius, c_s is the isothermal sound speed, and α is the viscosity parameter, which is usually assumed to be of the order of 10^{-2} in protoplanetary disks.

As a first approximation for calculating the disk thermal structure of the disk, we assume thermal coupling between dust and gas. This assumption is well justified for optical depths $\tau \geq 1$, as was shown by the disk models with detail thermal balance (Aikawa & Nomura 2006; Jonkheid et al. 2006). Sedimentation and coagulation of grains influence the disk temperature via a decrease in dust opacities (Birnstiel et al. 2009), which makes the atmosphere more transparent and hotter, and shifts the $\tau = 1$ surface deeper into the disk. The investigation of the response of the disk thermal structure on dust evolution is a separate problem, which will be addressed by future papers in this series.

The disk structure is calculated with a simplified version of the disk model described by D’Alessio et al. (1998) and D’Alessio et al. (1999). Unlike D’Alessio et al., in the calculation of gas temperature we take into account only two heating sources, namely, viscous dissipation and disk irradiation by the central star. Comparison of our disk models with the D’Alessio et al. results shows that this simplification does not significantly alter the derived disk physical structure, and thus modeling of the disk chemistry is not affected.

The following equations are used to describe the disk vertical structure:

$$\frac{dP}{dz} = -g\rho, \quad (1)$$

$$\frac{dT}{dz} = -\frac{3\kappa\rho F}{4acT^3}, \quad (2)$$

$$\frac{dF}{dz} = \frac{9}{4}\alpha P\Omega(R) + \Gamma_{\text{irr}}. \quad (3)$$

Here P is the gas pressure, g is the acceleration due to gravity, ρ is the gas density, T is the gas temperature, F is the flux of the thermal disk emission, $\Omega(R)$ is the disk (Keplerian) angular velocity at a distance R from the central object. The first term on the right hand side of Eq. (3) gives the viscous heating of the disk, while Γ_{irr} is the heating rate due to disk irradiation by the central object.

The two-dimensional structure of the disk is modeled in the so-called 1+1D approximation. It is assumed that at each radius the disk is in hydrostatic equilibrium (Eq. 1). Thus, the vertical structure of the disk can be found from the solution of equations (1–3) independently at each R . To calculate the disk temperature at each vertical slice, we integrate the transfer equation (2). The disk itself is described by the following parameters:

- accretion rate \dot{M} ;
- viscous parameter α ;
- temperature, radius, and mass of the central object T_*, R_*, M_* (radiation is assumed to be that of a black body);
- inner and outer disk radii R_{in} and R_{out} .

The outputs of the model are gas surface density distribution $\Sigma_{\text{gas}}(R)$, and the 2D density and temperature structure of the gas. The strengths of the UV and X-ray fields over the disk can then be calculated using the information about the gas and dust properties in the disk.

Using this model, we simulated a DM Tau-like system. The system has a disk with an outer radius of 550 AU, an inner radius of 0.03 AU, an accretion rate $\dot{M} = 2 \cdot 10^{-9} M_{\odot} \text{ yr}^{-1}$, and a viscosity parameter $\alpha = 0.01$. The disk is illuminated by UV radiation from the central star with an intensity $\chi = 500$ at $R = 100$ AU in units of the mean UV field of Draine (1978) and by the interstellar UV radiation. Two representations for the stellar UV field are used. One is the scaled Draine field, and another one is the representative observed

spectrum as discussed by Bergin et al. (2003). The effect of these different radiation fields will be discussed in section 3.1.

The star is assumed to have an X-ray luminosity of 10^{30} erg s $^{-1}$ (Glassgold et al. 1997). X-rays induce the same reactions as cosmic ray particles, so that X-ray ionization rate is in fact simply added to cosmic ray ionization rate. The disk mass is $M = 0.055 M_{\odot}$. The disk surface density profile and its power-law approximation are depicted in Fig. 1. The best-fit line has a slope of 0.84, which is somewhere in between of the Minimum Mass Solar Nebula index (1.5) (Weidenschilling 1977; Hayashi 1981) and the value derived for PPDs from SED at millimeter wavelengths, (≥ 0.5) (Andrews & Williams 2007). The density and thermal structure of the disk are shown in Fig. 2. The main model parameters are listed in Table 1. We do not consider a disk region beyond R_{out} .

2.2. Dust evolution in the disk

Several authors have constructed theoretical models for grain growth in protoplanetary disks (e.g. Nakagawa et al. 1981; Schmitt et al. 1997; Weidenschilling 1997; Dullemond & Dominik 2005; Ormel et al. 2007; Zsom & Dullemond 2008; Brauer et al. 2008b). The main challenges of grain growth modeling are the following: first, growth from $\sim 0.01 \mu\text{m}$ grains to centimeter-sized grains encompasses many orders of magnitude. A growth simulation must be able to conserve mass, since large particles can grow by accreting large numbers of very small grains. Second, particle size is not the only parameter determining the properties of grains: porosity, composition and the various possible outcomes of collisions further extend the parameter space (see Schmitt et al. 1997; Güttler et al. 2010).

Here, we use a slightly modified version of the code presented in Birnstiel et al. (2010) (see also Brauer et al. (2008b)). This is a statistical, mass-conserving code which implicitly solves the Smoluchowski equation, taking coagulation, fragmentation and cratering into account. It is important to note that we ignore radial drift of dust particles in the present study.

The mathematical formalism of the model is the following. The number density distribution $n(m, r, z)$ is a function of mass m , radius r , height z above the midplane, and time. We do not consider grain porosity as an additional parameter. We define the vertically integrated number density per mass m as

$$N(m, r) \equiv \int_{-\infty}^{\infty} n(m, r, z) dz. \quad (4)$$

We assume that coagulation and fragmentation Kernels K and L (defined below) are

independent of z . We can now describe the time-evolution of this distribution by a vertically integrated version of the Smoluchowski equation,

$$\begin{aligned}
 \frac{\partial N(m)}{\partial t} = & + \int_0^{m/2} N(m') N(m - m') K(m', m - m') dm' \\
 & - \int_0^\infty N(m') N(m) K(m, m') dm' \\
 & + \frac{1}{2} \int_0^\infty \int_0^\infty N(m') N(m'') L(m', m'') S(m, m', m'') dm' dm'' \\
 & - \int_0^\infty N(m') N(m) L(m, m') dm',
 \end{aligned} \tag{5}$$

where the radial dependence has been omitted, since we treat each radius independently, neglecting radial movement of dust. The right-hand side terms of Eq. 5 (from top to bottom) correspond to gain and loss by coagulation and gain and loss through fragmentation.

The coagulation kernel $K(m, m')$ and the fragmentation kernel $L(m, m')$ are then given by,

$$\begin{aligned}
 K(m, m') &= \frac{1}{\sqrt{2\pi(h(m)^2 + h(m')^2)}} \cdot p_c \cdot \sigma(m, m') \cdot \Delta u(m, m') \\
 L(m, m') &= \frac{1}{\sqrt{2\pi(h(m)^2 + h(m')^2)}} \cdot p_f \cdot \sigma(m, m') \cdot \Delta u(m, m'),
 \end{aligned} \tag{6}$$

where p_c and p_f are the coagulation and fragmentation probabilities, respectively, which have a sum of unity, $\Delta u(m, m')$ is the relative particle velocity, and $\sigma(m, m')$ is the sum of their geometrical cross sections. In this work, we consider Brownian motion, vertical settling (see Brauer et al. 2008b), and turbulent motion (see Ormel & Cuzzi 2007) as physical effects that produce the relative particle velocities.

Particles colliding with a relative velocity higher than the critical velocity u_f are assumed to fragment into a power-law size distribution of fragments (i.e., $S(m, m', m'') \propto m^{-1.83}$, see Brauer et al. 2008b) if the particle masses differ by less than one order of magnitude. Otherwise, the smaller body is assumed to excavate mass from the larger one by cratering, where the amount of excavated mass equals the mass of the smaller body. The fragmentation velocity u_f is taken to be 10 m/s (Birnstiel et al. 2009).

This model is related to a model of gas disk structure through two input parameters: radial midplane temperature distribution $T_{\text{mid}}(R)$ and the radial gas surface density distribution $\Sigma_{\text{gas}}(R)$. A more comprehensive description of the physics of coagulation/fragmentation and of its numerical implementation can be found in Brauer et al. (2008b) and Birnstiel et al. (2010).

The numerical model described above provides us with surface densities of grains of different masses. To calculate the vertical distribution $\rho_i(R, z)$ of grains, we assume that it is controlled by the equilibrium between gravitational settling and turbulent stirring, as proposed by Dullemond & Dominik (2004). Vertical scale heights are computed separately for each size bin.

2.3. Average grain size for the chemical model

An output of the dust evolution model is the grain size distribution at each disk location. In principle, this distribution can be incorporated into the chemical model by considering surface reactions and gas-dust interactions for each size bin separately. However this would make the model too complicated, and we elect to use a single grain size $\bar{a}(r, z)$ in the chemical model, which is computed from the equilibrium local grain size distribution in each disk location. The averaging is performed in a way which preserves the total surface area and the total dust mass. For a grain size distribution $f(a, r, z)$, where $f(a, r, z)da$ is the number of grains with radii between a and $a + da$ in the disk point with circumstellar radius r and height above midplane z , this means that

$$\frac{4}{3}\pi\bar{a}^3(r, z)\bar{n} = \frac{4}{3}\pi \int_{a_{min}}^{a^{max}} f(a, r, z)a^3 da, \quad (7)$$

$$4\pi\bar{a}^2(r, z)\bar{n} = 4\pi \int_{a_{min}}^{a^{max}} f(a, r, z)a^2 da, \quad (8)$$

where \bar{n} is the total number density of “representative” equal-sized particles. By dividing Eq. (7) by Eq. (8) one obtains

$$\bar{a}(r, z) = \frac{\int_{a_{min}}^{a^{max}} f(a, r, z)a^3 da}{\int_{a_{min}}^{a^{max}} f(a, r, z)a^2 da}. \quad (9)$$

An ensemble of grains with the mean radius $\bar{a}(r, z)$ has the same mass and total surface area as the original ensemble. We use $\bar{a}(r, z)$ exclusively in our astrochemical model described below when dealing with gas-grain interactions and surface chemical processes.

It is important to note that the way we calculate the average grain size is different from those usually used in works on grain growth (e.g., Brauer et al. (2008b); Birnstiel et al. (2010) etc.). In such works, the averaging is mass-weighted, i.e., emphasis is put on the size of a small fraction of the most massive grains. In this paper, on the other hand, averaging is surface-weighted, i.e. emphasis is put on a population of small grains which dominate the

grain surface area as well as the total number of grains. In other words, if simulations of grain growth would give us a distribution of grains in which a small number of big boulders co-exists with a big number of tiny grains, the average grain size of such a distribution calculated with expression (9) will be close to the size of small grains, contrary to the “usual” definition of average grain size.

3. Chemical model of the disk

In principle, simultaneous modeling of the disk chemical evolution, together with grain evolution, requires a non-local approach. Grains not only grow, but also move within the disk due to sedimentation and radial drift (Brauer et al. 2008b, e.g.), bringing with them molecules in icy mantles. However, a coupled chemo-dynamical disk model with grain growth would be computationally expensive, and difficult to analyze from the chemical point of view, so in the present study we choose to neglect transport effects. Thus, we model a chemical structure in the disk, taking dust properties and physical conditions from the previously-described disk model, and assuming that these conditions do not change over the timespan of chemical evolution considered. This timespan is taken to be 2 Myr, but the particular choice does not significantly affect our conclusions, as the abundances of most species are equilibrated very fast.

In this study, we utilize the chemical model described in Vasyunin et al. (2008). Initial elemental abundances are taken from Table 1 in Vasyunin et al. (2008). Compared with the original chemical model, we made several modifications. First, dissociative recombination of ions on grain particles is included according to Umebayashi & Nakano (1980) and Semenov et al. (2004). Second, for gas-grain chemical interactions and grain surface reactions, we used variable dust-to-gas mass ratios and the average grain size calculated at each disk point using data from the grain growth model. For grain surface reactions, we utilized model H from Vasyunin et al. (2009). In this model, only thermal hopping is a source of mobility of surface species, and a high diffusion-to-desorption energy ratio of 0.77 is adopted for all species. Under these conditions, stochastic effects in grain surface chemistry are negligible and classical rate equations may be safely used (Vasyunin et al. 2009; Garrod et al. 2009). In our model molecular hydrogen is formed via the surface reaction $\text{H} + \text{H} \rightarrow \text{H}_2$. The rate of this reaction, as well as of other surface reactions, is calculated according to the formalism described by Hasegawa et al. (1992). The rates are inversely proportional to the surface area of an individual dust grain.

The cosmic ray ionization rate has been adopted according to Eq. 19 from Sano et al. (2000). The unattenuated cosmic ray ionization rate was taken to be $1.3 \cdot 10^{-17} \text{ s}^{-1}$. The

final and most important change is the detailed treatment of photoprocesses which take into account the shape of the UV spectrum of the central star, and its attenuation in the disk due to absorption of the UV photons by dust grains (see Section 3.1). Below we discuss in detail the treatment of these photoprocesses.

3.1. Photoreactions

Photoreactions represent the crucial element of chemical networks designed for the upper disk atmosphere, and it is this element that is most affected by the dust evolution. In the conventional approach, photoreaction rates are estimated as

$$k^{\text{ph}} = \chi k_0 \exp(-\gamma A_V), \quad (10)$$

where k_0 is the reaction rate for the unshielded interstellar UV radiation field, χ is the UV intensity scaling factor, and γ is a parameter used to account for the different dust extinction in the UV and visual wavelengths. Generally speaking, A_V estimated from the gas column density cannot be used in this case, because it is based on a particular choice of dust properties (opacities and dust-to-gas mass ratio), and on the assumption that these properties do not vary in the medium. In our study dust parameters are position-dependent, so we have to be more careful. To compute rates of photodissociation and photoionization one uses the general expression:

$$k^{\text{ph}}(r, z) = 4\pi \int \frac{I_\nu(r, z)}{h\nu} \sigma_\nu d\nu, \quad (11)$$

where the mean UV field intensity $I_\nu(r, z)$ is obtained as a solution of the radiation transfer problem. In this study we adopt a simplified approach, in which $I_\nu(r, z)$ is given by the equation

$$I_\nu(r, z) = I_\nu^{\text{st}}(r, z) \exp(-\tau_\nu^{\text{st}}(r, z)) + I_\nu^{\text{D}} \exp(-\tau_\nu^{\text{IS}}(r, z)), \quad (12)$$

where $I_\nu^{\text{st}}(r, z)$ is the unattenuated diluted stellar radiation field, I_ν^{D} is the so called Draine radiation field (Draine 1978). We investigated two representations for the stellar radiation field. In the first representation the observed spectrum for TW Hya is used, scaled in such a way that the integrated UV intensity is about 500 in units of the Draine field at 100 AU from the star (Bergin et al. 2003). A combination of FUSE (Herczeg et al. 2002) and HST (Ayres 2010) data is utilized, and the resulting spectrum is shown in Fig. 8. Essentially, this spectrum is very close to the one used in Bergin et al. (2003). In another representation, the stellar radiation is assumed to be given by the scaled Draine interstellar field, with the same normalization. Comparison of results for the two representations shows that both spectra lead to the same general conclusions about the chemical structure of the disk both

with evolved and unevolved dust. This is consistent with findings of van Zadelhoff et al. (2003). These authors compared molecular distributions and column densities for the cases when the UV spectrum is given either by the scaled ISFR spectrum or the smoothed TW Hya spectrum and found no significant differences (their models A and B). In our case, the relative similarity of results for the two representations is caused by effective attenuation of the stellar radiation in the disk, so that the radiation field is in both cases dominated by the interstellar field everywhere in the disk, except for the uppermost layers. The situation would have been different if scattering were present in our model. When the scaled ISRF is used to represent the stellar radiation, scattering is in some sense equivalent to just a somewhat different scaling factor for the vertically penetrating radiation. However, when a more realistic stellar spectrum is used, like the $L\alpha$ -dominated TW Hya spectrum, scattered stellar radiation would noticeably change photoreaction rates for species with large cross-sections in the $L\alpha$ range (Bergin et al. 2003). Note that van Zadelhoff et al. (2003) did find a significant dependence on the spectrum of the radiation field in a more general sense, that is, for the case when no UV excess is taken into account at all (their model C).

Also, van Zadelhoff et al. (2003) investigated how different approaches to the radiation transfer, namely, full 2D and simplified calculations, such as described below, impact the chemical composition of a protoplanetary disk. They found that column densities of most species are not sensitive to the chosen approach. Important exceptions are the molecules CN, C_2H , CS and HCN, but only in the inner disk. Their column densities do significantly depend on the adopted UV radiation transfer model. However, in our model, the strength of the stellar UV field is more than an order of magnitude weaker than that considered by van Zadelhoff et al. (2003).

The optical depth $\tau_\nu^{\text{st}}(r, z)$ is computed along the ray between the star and the current location, so that

$$\tau_\nu^{\text{st}} = \int \kappa_\nu(r, z) \rho(r, z) ds. \quad (13)$$

Dust sedimentation is taken into account in the dust density $\rho(r, z)$. The absorption coefficient $\kappa_\nu(r, z)$ per unit dust mass is calculated at each location along the ray as

$$\kappa_\nu(r, z) = C \int da f(a, r, z) Q(a, \nu) \pi a^2, \quad (14)$$

where the normalization coefficient C is defined by the condition

$$1 = C \int da f(a, r, z) \frac{4}{3} \pi a^3 \rho_d. \quad (15)$$

Absorption efficiency factors $Q(a, \nu)$ are taken from Draine & Lee (1984) and Weingartner & Draine (2001). For the purpose of opacity computation, we assume that dust consists of silicate and

carbon (graphite) components contributing, correspondingly, 70% and 30% to the total dust mass density (Weingartner & Draine 2001). In Eq. 15 ρ_d is the density of dust material, taken to be 3 g cm^{-3} for silicate grains and 2.24 g cm^{-3} for graphite grains. In the expressions above, $f(a, r, z)$ is the local evolved grain size distribution that comes from the dust growth and sedimentation model. Considering coagulation and fragmentation, we do not distinguish between the two materials as experimental data show a similar dust evolution behavior for both types of grains (J. Blum, private communication).

The optical depth $\tau_\nu^{\text{IS}}(r, z)$ is computed in the same way, but in vertical direction from the disk surface to the height z .

The reaction cross sections are taken from van Dishoeck et al. (2006) and supplemented with the additional data for the Ly α wavelength, with the exception of the photodissociation cross sections for NO, HCN, NO₂, SO₂, OCS, NH₃, CH₄, H₂O₂, and C₂H₂. For these molecules, monochromatic photodissociation cross sections from the AMOP² database have been used in our study.

To compute the rates of photoreactions for which wavelength-dependent cross-sections are not available, we use the standard expression (10), however with the modified procedure for computing A_V . The conventional expression for optical extinction

$$A_V = N_H / 1.59 \cdot 10^{21} \text{ cm}^{-2} \quad (16)$$

is valid for dust which is well-mixed with gas and consists of single-sized grains (10^{-5} cm) and a dust-to-gas mass ratio 0.01, but it can easily be re-normalized for other values of these parameters. We integrate A_V along the ray between the star and the considered location (or in a vertical direction for interstellar radiation), taking into account the variable dust-to-gas ratio along the ray, and a variable average grain size $\bar{a}(r, z)$.

Self-shielding for H₂ photodissociation is computed using the Draine & Bertoldi (1996) formalism, with the modified A_V value used to account for dust attenuation. The self- and mutual shielding for CO photodissociation is computed with data from Lee et al. (1996). Their dust attenuation is not included in the resultant shielding value, as it is replaced by our optical depths. To compute self-shielding factors, one would need to know the CO column density along the ray, which in the chemical study would entail iterations. We adopted a much simpler approach, assuming that CO self-shielding is proportional to the overall column density with an average abundance of 10^{-6} . To check whether this simplification affects our conclusion, we run two models, bracketing possible self-shielding values. In one of

²<http://amop.space.swri.edu/>

the models, maximum self-shielding is assumed which would correspond to all C atoms being in CO molecules. In the other model, CO self-shielding is assumed to be zero. Comparison of these two models showed that various treatments of self-shielding do not change our main conclusions while they do change some numbers, so we believe that the use of this simplification is acceptable. Anyway, species that turned out to be sensitive to the CO self-shielding treatment (CS and H₂CO) are not included in Tables 2 and 3.

In the model, several important simplifications are made. First, we assume that dust and gas temperatures are equal everywhere in the disk. Next, we neglect transport processes, such as radial and vertical mixing, and their influence on molecular abundances. Finally, when simulating grain-surface chemistry, we utilize the single average grain size instead of the real grain size distribution. Impact of these simplifying assumptions on the results of this study is discussed in Section 5.

4. Results

4.1. Dust evolution in the disk

Using the model of grain growth and fragmentation described in Section 2.2, we calculated the evolution of surface densities for grains of different sizes, starting from the standard MRN grain size distribution at $t = 0$. (Mathis et al. 1977). Snapshots of surface density as a function of grain size for four time moments are shown in Fig. 3. The corresponding vertically integrated average grain size calculated according to Eq. (9) using vertically integrated number densities from Eq. (4) is shown in Fig. 4.

The two peaks in Fig. 4 appear because small grains typically grow together in a more or less uniform bump moving to larger sizes. So, the whole distribution shifts up in size until grains reach the fragmentation barrier. Once that happens, most of them fragment, and the small sizes get re-populated. The average grain size drops again, and an equilibrium between growth and fragmentation is established.

Since the disk density is higher closer to the star, grain growth proceeds faster there (in our model we do not consider the radial drift of grains). One can see that at $R \leq 30$ AU a steady-state in the grain surface density distribution is reached within less than 10^4 yrs. However, in the outer disk ($R \geq 100$ AU) grain surface density evolves much slower. A steady-state distribution is barely reached there within 10^6 yrs. In order to ensure that grain parameters are equilibrated at all radii, we ran the grain evolution model for 2 Myr.

It is important to point out that the highest surface density (Fig. 3) corresponds to

grains which are bigger than the average particle size, as shown in Fig. 4. It is in these large grains that most of the dust mass is contained, while small grains dominate the dust surface area. Therefore, the presence of small grains in the disk mediates the net effect of grain growth from the point of view of gas-grain interactions, as they depend primarily on the available grain surface.

In general, the grain growth is quite modest in the modeled disk. The largest increase in the surface averaged grain size is achieved in the inner disk midplane ($10 \leq R \leq 100$ AU) with a mean grain size of 10^{-4} cm ($1 \mu\text{m}$). In the outer disk region ($R \geq 100$ AU) the average grain radius increases relative to the initial value by a factor of only 3–5.

In contrast, differential dust settling seems to be much more significant. 2D distributions of the total dust-to-gas mass ratio and average grain size are shown in Fig. 5. Dust settling reduces the dust-to-gas mass ratio in disk regions above the midplane. Everywhere above $Z/R \sim 0.1$ this ratio is significantly below the canonical value of 0.01. In the chemically rich intermediate layer it varies between 0.001 and 0.01, while in the disk atmosphere it drops down to $10^{-4} - 10^{-5}$. At the same time, in the midplane the dust-to-gas mass ratio can reach a value of 0.02. Similarly, the average grain radius decreases above the midplane, though its change is not that dramatic. In the disk atmosphere, the average grain radius is only 10^{-6} cm ($0.01 \mu\text{m}$), because large grains efficiently settle down to the midplane.

Summarizing both the vertically-averaged and 2D parameters of the evolved dust, we note that the overall effect of the grain growth and sedimentation in our disk model is the global decrease of the total surface area of dust grains (see Fig. 6). This is less pronounced in the outer part of the disk ($R \geq 100$ AU), corresponding to a factor of only 2–3. In the inner disk region ($R \leq 100$ AU) the decrease of the dust surface area is more prominent, i.e., up to one order of magnitude. The ratio of evolved to original grain surface area has a steeper radial dependence than variations in the vertical direction. This is because the decrease in total dust surface area above the midplane, caused by the dust settling, is partly compensated by the presence of small particles dominating the surface area.

4.2. UV field in the disk

For the radiation field in the disk, we consider three basic models. In model A5, all grains are assumed to have a single size of 10^{-5} cm. This is the model of choice in most astrochemical computations. Model A4, in which all grains have the same radius of 10^{-4} cm, can be considered a rough representation of grain growth (without sedimentation). Finally, in model GS both grain growth and sedimentation are taken into account fully. For brevity

we will call the GS and A4 models “evolved”, while the A5 model is referred to as the “standard” model.

In all models, the disk is illuminated by both stellar and interstellar UV radiation. For disk chemistry, the strength and shape of the UV field is of primary importance, as it controls the rates of photoionization and photodissociation, as well as the efficiency of the photodesorption of grain mantles (e.g., Bourdon et al. 1982; Westley et al. 1995; van Zadelhoff et al. 2003; Öberg et al. 2007). Due to the presence of dust, the UV field is attenuated as it penetrates deep into the disk. As mentioned in the introduction, the attenuation of starlight in the disk atmosphere can also be caused by PAH particles. IR observations of protoplanetary disks show that PAHs are an abundant component of some disks around Herbig Ae stars (e.g., Acke et al. 2010), but they are usually not seen in the spectra of T Tauri stars (Geers et al. 2006). Therefore, for simplicity, we neglect their possible contribution to the opacity and heating of the disk.

In Fig. 7, the distribution of the integrated UV field strength over the disk is shown in logarithmic scale. Contours are labeled in units of the interstellar UV radiation field (Draine 1978). In the evolved models the disk becomes more transparent to the incident UV radiation. While in model A5 (Fig. 7, middle panel) one can clearly see the dark zone at the disk midplane (up to $Z/R = 0.15$), this region is significantly smaller in models GS and A4. On the other hand, in evolved models, the midplane can be divided into two parts. The inner part at $R \leq 100$ AU remains as opaque to UV radiation as in the standard model, while the outer midplane can hardly be called “dark”, because of the smaller opacities in models GS and A4. In model A4, the UV strength in this region is $\sim 10^5$ times higher than in model A5. Thus, the outer disk in model A4 consists of only two layers: the atmosphere and the moderately UV-illuminated midplane (Fig. 7, left panel). In the GS model the outer disk is not that transparent, even though the inner dark region of the midplane is still narrower than in model A5. The UV strength in the outer disk region is higher than in model A5 by a factor of $10 - 10^3$, and is only a small fraction of the UV strength in the intermediate layer. Therefore, the three-layered disk chemical structure is preserved in the GS model but the midplane is only “dim” rather than “dark” (Fig. 7, right panel).

The UV spectrum at various heights above the midplane for a disk radius of $R = 100$ AU is shown in Fig. 8. For illustrative purposes, we also schematically include the Ly α feature. As expected, the dust absorption is stronger at shorter wavelengths. It is important to note that Ly α feature “disappears” in the densest part of the disk, due to the strong absorption and the absence of any efficient scattering mechanisms for UV photons in our model. Hence, we expect only minor differences in column densities of molecules in the current version of our model with and without Ly α , because the major contribution to column densities comes

from the densest parts of the disk. In future works, we plan to treat the scattering of Ly α photons (see Bergin et al. 2003).

Another factor that can affect the UV field in the upper disk atmosphere is the gas-phase opacity. Recently, Bethell & Bergin (2009) noted that water and OH molecules can be a source of significant absorption in the UV band. However, to take this effect into account properly, one would need to model chemical and physical disk structure self-consistently.

4.3. Chemical structure of the disk

We now want to discuss which effects – grain growth or sedimentation – are dominating changes in column densities of the various gas phase species. Note, that in all three basic models detailed cross-sections are used, to calculate photoreaction rates whenever possible (see section 3.1).

4.3.1. Inner disk: models GS and A5

First, we compare models GS and A5. The overall trend for these two models is that the column densities in the inner disk are greater for most species (like CO, CO₂, NH₃) in the GS model than in the A5 model, sometimes by orders of magnitude. Of all the gas-phase species, only 10% have greater column densities in the A5 model at $R = 10$ AU (like S⁺, HNO, CP). This result may seem counterintuitive, as the disk which is transparent to UV radiation should represent a more hostile environment for molecules. However, at the same time the growth of dust particles decreases their total surface area, thus lessening the effectiveness of mantle formation and surface chemical processing. Also, the more intense UV field in the upper disk causes faster photodesorption, shifting the balance between sticking and desorption toward higher gas-phase abundances.

The most dramatic example of this difference is H₂CS. The column densities of this molecule at 10 AU in models GS and A5 differ by almost 6 orders of magnitude. However, there are also less exotic examples represented by basic carbon compounds, also at 10 AU, where the effects of dust evolution are stronger. Both CO (see Fig. 9) and CO₂ are concentrated primarily in the warm molecular layer. The peak gas-phase abundances of CO are nearly the same in models GS and A5, as they are essentially equal to the total carbon abundance. However, the location of the peak of the relative abundance of CO in the GS model is shifted downward to the denser disk region causing the CO column density to increase. The peak of the CO₂ abundance is also located deeper in the GS model, and

the maximum abundance of this molecule is two orders of magnitude higher than in the A5 model. A similar behavior is characteristic to the abundances and column densities of N_2H^+ , NH_3 , and H_2O (see Fig. 10, fourth row). While in model A5 the column densities of these species decrease towards the inner disk, in the models with grain growth (A4 and GS) they are nearly constant. Again, this is a manifestation of the faster grain evolution in the disk interior with respect to the outer region ($R \geq 50 - 100$ AU).

In the inner disk midplane, where temperatures are low enough to allow icy mantle formation, all carbon atoms are locked in surface CO_2 . Midplane surface and gas-phase abundances of CO and CO_2 do not differ in models GS and A5. At the same time, in model A5 surface hydrogenation products of these species are significantly more abundant. For example, s- H_2CO and s- HCOOH (the prefix “s-” denotes surface species) are enhanced by one to two orders of magnitude in the model with “standard” dust properties.

Another noticeable difference between models GS and A5 is the layer of enhanced depletion located right beneath the molecular layer, which is clearly observed in the A5 model, and is absent (or at least less pronounced) in model GS. The origin of this depletion layer is related to hydrogen and helium ionization. This effect is most directly seen for CO . In the depletion layer, this molecule is rapidly destroyed in reactions with He^+ . Below this layer, helium is not ionized as X-rays do not penetrate there and this channel is not important. Above it, the reaction of CO with ionized helium cannot compete with rich ion-molecular chemistry. In the GS model, molecular freezing is less effective because of decreased available dust surface, and photodesorption is enhanced; thus formation of this depletion layer is suppressed. It is also important to note that cosmic ray (CR) and X-ray ionization is not affected by dust sedimentation in our model.

Abundant gas-phase water in the GS model consumes hydrogen ions effectively (produced by CR ionization and in reactions of H_2 with He^+), and their abundance drops significantly at intermediate heights (about 1.5 AU at $R = 10$ AU). Correspondingly, abundances grow for other species that would otherwise have been destroyed by H^+ . Among these species are some long carbon chains, like C_6H_2 , and cyanopolyynes, like HCN , HC_3N and HC_5N (Fig. 11, first and second rows). Conditions for the gas-phase synthesis of these compounds are only met in the narrow disk layer, and so the presence or absence of H^+ in this layer determines whether or not molecules with long carbon chains can be abundant in the inner disk. This is why their column densities are 4–5 orders of magnitude higher in the GS model, where they bind a significant fraction of C atoms, than in the A5 model.

Thus, the typical net effect of the dust evolution is to increase the gas-phase abundances (despite enhanced photodissociation) of most molecules, and to decrease abundances of their surface counterparts. Of course, given the intricate structure of chemical networks, the

response is not always straightforward, and there are species for which *both* gas-phase and surface abundances are increased in the GS model (like H₂S), and also species for which both gas-phase and surface abundances are decreased in the GS model (like HNO). Also, dust evolution suppresses surface hydrogenation and, in particular, formation of the simplest organic molecules in icy mantles.

4.3.2. Outer disk: models GS and A4

Yet another comparison, that is useful, is to compare the results of models GS and A4. An increased average grain size (as well as an increased upper limit of the grain size distribution) can be thought of as a simplified way of modeling grain growth. The main assumption in this representation is that dust evolves uniformly over the entire disk. As we have seen, this is not the case, so the largest deviations should be in those disk regions that are less affected by grain growth and sedimentation, (in regions further away from the star). Indeed, at a radius of 10 AU, the vertical abundance profiles in the GS and A4 models for most species are nearly identical, with most differences observed at $R > 100$ AU.

To illustrate features specific to model A4, we turn to the molecular disk content at 550 AU. The biggest differences in column densities are found for surface species, which is expected, as the grain surface area is much smaller in this model than in the other two models. Some complex species, like s-C₂O and s-C₃O, are underabundant in terms of column densities by more than 5 orders of magnitude in model A4. The column densities of other carbon-bearing surface species, like s-CO₂, formaldehyde, methanol, are 2–4 orders of magnitude smaller than in other models. On the other hand, the column densities of ices, which are not affected that much by surface chemistry (s-CO, s-H₂O, s-NH₃), differ only slightly in models GS and A4. This is largely because these molecules simply bind nearly all CNO atoms in both of these models.

For the gas-phase species, the largest difference in column densities is observed for N₂O. This molecule is overabundant (in terms of column densities) in model A4 relative to model GS by four orders of magnitude. Similar overabundance is also seen for other N-bearing species as well, like NO₂, OCN, and ammonia. While the network of chemical pathways connecting all these species is quite complicated, the underlying reason for their higher abundance seems to be simple. Surface transformations, which are less effective at this radius in model A4 than in model GS, lock somewhat fewer nitrogen atoms in surface ammonia making them available for various gas-phase species. It must be kept in mind that the column density of s-NH₃ is so high that even minor relative differences in $N(\text{s-NH}_3)$ between models A4 and GS significantly affects column densities of other, less abundant

N-bearing species. Similar trends are observed in other families as well. In general, we can say that dust acts as an irreversible (or nearly irreversible) sink for atoms, locking them in surface species with high desorption energy. As grains get bigger, their total surface area diminishes, and more atoms are available for richer gas-phase chemistry.

Column densities alone are not the unique indicator of a specific chemical structure. Even if the column densities of some molecules are almost the same in models GS and A4, their vertical distributions can be different in terms of both width and location of the molecular layer. In general, as we move from model A5 to GS to A4, at large radii, the molecular layer gets thinner, and is located deeper in the disk.

4.3.3. Comparison to other works

The chemistry in a disk with evolved dust was studied by Aikawa & Nomura (2006). In their investigation, H_3^+ was indicated as one of a few species sensitive to the grain growth in terms of a column density. In our study, model A4 is most suitable for the comparison with the model of Aikawa & Nomura (2006), and comparison of models A5 and A4 indeed confirms the statement made in their paper. However, H_3^+ behaves differently in our two evolved models (GS and A4; see Fig. 10, sixth row). In model GS the column density of H_3^+ does not significantly differ from that in model A5. As the formation of H_3^+ is driven by cosmic ray ionization of H_2 , with the same rate in all three models, the difference is related to the destruction of this ion. It is consumed mainly in dissociative recombination reactions with electrons and negatively charged grains as well as in ion-molecular reactions with CO, H_2O , CN, and other radicals. Therefore, the distribution of H_3^+ in the disk is controlled by fractional ionization and by the width and location of the molecular layer. In models GS and A5, peaks of molecular abundances are located at different heights, but still above the midplane. Because of this, the vertical profiles of the H_3^+ abundance in these two models are similar, except for a shift relative to the midplane. Consequently, the *column density* of H_3^+ is not sensitive to grain evolution as described by model GS.

On the other hand, in model A4 the molecular layer extends down to the midplane, and, thus, protonation reactions involving H_3^+ are active in a broader disk zone. The main channels of H_3^+ destruction in the outer disk are its reactions with CO and water, which are abundant even in the cold gas in model A4. This emphasizes the need of careful grain growth modeling in chemical studies, as an adopted approach to the grain evolution may affect conclusions even about some primary species.

The increase in many molecular column densities seen in model GS seems to be in

contradiction with the conclusion of Aikawa & Nomura (2006) that grain growth does not affect most column densities. However, they do not consider dust settling and also model dust growth by increasing the upper size limit, thus, keeping the significant amount of small grains. This means that the upper disk in their model is, probably, more opaque than our disk in model GS. Thus, the increase in column densities is only observed when dust growth and settling are considered simultaneously.

Our basic results compare favorably with those obtained by Jonkheid et al. (2004, 2007). However, the two models are also quite different. In particular, freeze-out and surface processes are not taken into account by Jonkheid et al., and also assumptions on the central star are very different from our work.

Nevertheless, the CO depletion layer is seen in both the T Tauri disk model and especially in the Herbig Ae/Be disk model, when dust is assumed to be well-mixed with the gas. As in our model, this layer disappears when dust settling is included in the modeling by Jonkheid et al. In both models, the peaks in the vertical distributions of molecular abundances occur closer to the midplane in the models with dust evolution.

In terms of column densities, however, the two models differ. In our model, as grains become larger, the molecular column densities become larger. The opposite trend is observed in the model by Jonkheid et al. (2007) (cf. their Fig. 8). But this difference is understandable: the disk in their model is warmer, because the central star is hotter and more luminous. As the disk becomes more transparent to UV radiation, molecular column densities drop. In our model, chemical interactions between gas and dust are very important, and the difference between column densities in different dust models is not controlled solely by photodissociation.

Another study to be compared with our results is those of Pascucci et al. (2009). These authors found that there is a significant underabundance of HCN relative to C_2H_2 in disks around cool stars and substellar objects. They attribute this underabundance to the differences in UV radiation field. The photodissociation of molecular nitrogen is less efficient in the vicinity of cool stars, so there are not enough free nitrogen atoms to be incorporated into HCN molecules, while N atoms are abundant around hotter stars with noticeable UV excess. The UV spectrum of the central object is the same both in GS and A5 models, however one of the main results of grain evolution is that the integrated UV field in the upper disk is stronger in model GS than in model A5, and we may expect a similar trend in the HCN abundance.

And we do see this trend in the outer disk (Fig. 10, fifth row and Fig. 11, first row). While in model A5 at $R > 100$ AU column densities of HCN and C_2H_2 are almost equal, in

model GS (with stronger UV field) HCN is 15 times more abundant than acetylene. Analysis of chemical reactions shows that enhanced HCN is indeed caused by greater abundance of N atoms. The trend is not preserved at smaller radii, though. At $R = 10$ AU in model A5 the column density of HCN exceeds that of acetylene by a factor of 42 (compared to near equality at greater distances). This is because in model A5, with abundant dust in the upper disk, surface HCN synthesis with subsequent desorption becomes an important factor increasing gas-phase abundance of this molecule.

One should keep in mind that both under- and overabundance of HCN relative to C_2H_2 in model GS is observed on top of the overall trend for column densities of most molecules to be greater in this model.

4.3.4. Fractional ionization in the disk

Dust evolution is reflected not only in the abundances of some molecules, but also shows up in a more integral way, affecting the fractional ionization x_e of the disk (see Fig. 10, bottom row). Since in our model one grain can adsorb not more than one electron, change of dust properties impacts disk ionization mainly through change of absorption of the UV field which is important for gas-phase chemistry. While the ionization degree exceeds 10^{-10} everywhere in the disk, grain number density is not more than 10^{-12} in respect to hydrogen nuclei. Therefore, ionization degree is controlled by cation chemistry while the contribution of electron sticking to dust grains is less than 1%. In the disk atmosphere differences are small as the entire ion content is provided by ionized carbon and ionized hydrogen (in the uppermost X-ray ionized layer). Deeper in the disk, different properties of dust cause x_e in models A5 and GS to differ by almost two orders of magnitude. This difference is primarily caused by different dominant ions at different heights. Let's consider a slice at $R = 100$ AU as an example. When absorption gets high enough so that C^+ is no more a dominant ion ($z \lesssim 40$ AU), in model GS most electrons are provided by metals. Sodium, magnesium, and iron ions stay dominant down to $z \sim 15$ AU. Below this level, where most dust is concentrated in model GS, metals are depleted, and most abundant ions are H^+ and H_3^+ (in almost equal shares).

In model A5 dust is equally abundant everywhere in the disk, and metals are depleted at all heights below 40 AU. Correspondingly, almost all ions at these heights are provided by H^+ and H_3^+ . These species are heavily involved in ion-molecular chemistry, so their abundances are very sensitive to the overall molecular content. In particular, ionized hydrogen is effectively consumed in reactions with ammonia, water, hydroxyl etc. These species are abundant in the warm molecular layer ($z \sim 30$ AU) and depleted right below it ($z \sim 20$ AU).

Correspondingly, in the warm molecular layer H_3^+ is the most abundant ion, while at lower heights the balance shifts toward H^+ . The equilibrium fractional ionization (for a single ion) is inversely proportional to the square root of the recombination coefficient. This coefficient is significantly lower for H^+ than for H_3^+ , so the fractional ionization is higher at $z \sim 20$ AU, where H^+ dominates.

5. Discussion

5.1. Disk chemistry as a tracer of grain evolution

Can molecular abundances in a protoplanetary disk be tracers of grain evolution? Since the distance to the Taurus-Auriga complex, where most known disks around low-mass pre-main sequence stars are located, is ~ 140 pc (Elias 1978) and the expected angular resolution of ALMA is up to $0''.01$, the spatial resolution of disk observations should be $\sim 1\text{--}2$ AU. This is sufficient to study the spatial distribution of molecular abundances in the outer disk (10–600 AU). So it is worthwhile to ask if there are species, sensitive to the grain growth at a level that would make them detectable tracers of this process. An immediate product of observations are molecular lines. Therefore, we need to predict not abundances or column densities, but the shapes and intensities of molecular lines, as well as the variations caused by grain evolution (e.g., Semenov et al. 2008). The physical model of the disk employed in this study is quite simple, however, so it does not make sense to perform realistic radiative transfer modeling. In this situation, we have chosen to consider only given species as a possible grain evolution tracer if its column density differs in models A5 and GS by an order of magnitude or more in at least one of representative radial regions around 10 AU, 100 AU and 550 AU. An exception is made for CO, which has a very high column density. In the inner disk and at $R = 100$ AU from the star CO column density becomes higher by a factor of 5–7 in model GS in comparison to model A5.

Major species, both sensitive and insensitive to grain evolution in our model, are grouped in Tables 2 and 3 respectively. Additionally, Table 2 shows the observed column densities for several species, taken from Semenov et al. (2004) (except for HCO^+ and N_2H^+ which are taken from Table 3 in Dutrey et al. (2007) and C_2H which is taken from Henning et al. (2010)). It is clear that the column densities of species which have already been observed in disks so far, do not seem to be strongly influenced by the changing dust properties at large distances from the star, i.e., in the domain of single-dish observations. Closer to the star, however, the differences are more significant. Specifically, at $R=10$ AU, the column density of water in model GS exceeds that in model A5 by a factor of 560. A word of caution is to be said about water abundance. While column densities for all other molecules have

reasonable values in our models (as compared to available observations), water seems to be an exception. Recent Herschel results (Bergin et al. 2010) show no observable water lines in the DM Tau spectrum. Bergin et al. (2010) estimated the upper limit for the water column density in the outer disk to be about $3 \cdot 10^{13} \text{ cm}^{-2}$, which is much lower than the water column density in our models. They suggested that low water abundance may serve as an indication of grain growth and sedimentation. However, as we said previously, our model do not predict significant grain evolution in the outer disk, so the DM Tau disk may represent a later stage of the grain growth than our model.

Of course, not only abundances (i.e., column densities) themselves, but also their ratios, can be an indicator of the grain growth. However, as in the example of HCN and C_2H_2 , considered above, and motivated by observations by Pascucci et al. (2009), the influence of the grain evolution on the abundance ratio can be at least twofold, and calls for a more detailed consideration.

Another pair of observed species that may potentially be useful as a tracer of the grain evolution is HCO^+ and N_2H^+ (Dutrey et al. 2007). While the average column densities of these species in model GS agree quite well with observations of Dutrey et al. (2007), the ratios of their column densities in models GS and A4 are quite different: at $R = 550 \text{ AU}$ the ratio $N(\text{HCO}^+)/N(\text{N}_2\text{H}^+)$ is 150 in model GS, and 1500 in model A4. While the main focus of our work was on comparison between models GS and A5, not between models GS and A4, the difference mentioned here shows that this ratio is worth checking in a more detailed model.

At the disk periphery, where dust evolution is least prominent, the only species that is sensitive to dust growth and sedimentation on the level of an order of magnitude is methanol. However, the methanol column density is quite modest ($2 \cdot 10^{11} \text{ cm}^{-2}$) and even smaller closer to the star.

In general, we may conclude that the chemical signatures of early grain evolution are hardly observable with single-dish instruments, although they are a promising target for highly sensitive interferometers such as ALMA.

The composition of the icy mantles of dust grains in the disk also may provide information about the grain evolution process. Terada et al. (2007) showed that it is possible to assess the mantle composition through observations of scattered light in edge-on disks around T Tau stars. They found deep water-ice absorption lines corresponding to an optical depth of $\tau=1$ in the directions of edge-on disks HK Tau B and HV Tau C. In order to check whether ices in the observed region are sensitive to the grain evolution process, we calculated the mantle composition in models A5 and GS near the optical disk surface $\tau = 1$ (see Table

4). Due to the different dust properties in models A5 and GS, the location of this surface is different in the two models. It is closer to the midplane in model GS, where the disk is more transparent to UV radiation than in model A5, where the dust is pristine and more opaque. The vertical temperature gradient of the dust is the most important factor in determining the differences in the ice composition between the two models. Since our model of the vertical structure of the disk is not self-consistent, the temperature at the $\tau = 1$ surface is determined only approximately. Therefore, differences in the chemical composition of ices in models A5 and GS should only be considered as qualitative in nature.

In the inner disk ($R = 10$ AU), the temperature at its optical surface is 50 K in model GS, and 80 K in model A5. At this temperature range, the ice composition is totally dominated by water ($\sim 99\%$). Ammonia is the second most abundant ice compound ($\sim 1\%$), and other species are present in ice only in trace amounts. At a disk radius of 100 AU, the ice composition at $\tau = 1$ is significantly different in models A5 and GS and relatively complex. While water is still the dominant ice constituent, it shares this role with hydrocarbons C_nH_m , which are produced efficiently by both surface chemistry and gas-phase chemistry in this disk region. Also, in the GS model, several other species, such as CO_2 , H_2CO , HCN etc. stay in ice in noticeable amounts. Further away from the star, at a radius of 550 AU, the ice composition in models A5 and GS is almost the same again because the optical surface at this distance in both models corresponds to very similar temperatures of approximately 30 K.

Such differences in grain mantle composition at the optical surface of the disk may serve as an additional tracer of the grain evolution process. However, the results described above should be confirmed with detailed, self-consistent models of the vertical structure of the disk.

5.2. Model limitations and future work

We have already mentioned that column densities are only a partial indicator of grain growth. Line emission modeling is needed to assess observable tracers of dust evolution with more confidence. But, there are some issues that need to be addressed prior to this modeling. As we mentioned in the introduction, the simplified setup of our model allows us to isolate the chemical outcomes of grain evolution, although the process of grain growth should probably have some more general influence on the disk structure. The response of a disk to dust evolution has already been addressed a number of times but with only an oversimplified approach to grain growth and/or sedimentation. Our modeling shows that dust evolution in a disk is highly non-uniform, both in the vertical and radial direction, which should be reflected in disk physical properties.

In future disk models, one would need to at least calculate the processes of grain growth and sedimentation consistently with the description of the disk structure, as density and temperature distributions in the disk are controlled by opacities. Dust absorption is definitely affected by growth and sedimentation, but both these processes, in turn, depend on the disk structure. In this study, changes in the surface-averaged grain size (and, hence, in the total grain surface area) are only minor, and even in model GS, where dust is evolved, the disk is relatively opaque to the incoming radiation. This means that extra heating due to decreased opacity would mostly affect the upper disk, above the region where most molecules are concentrated. As in this region molecular abundances are mostly controlled by photoprocesses, most column densities probably will not be strongly affected by the increased gas scale height or gas temperature in the upper disk. The exception is represented by abundant components that bind almost all CNO atoms in the molecular layer (CO, N₂, O). As we noted, the increase of their column densities in the inner disk in models GS and A4 relative to A5 is partially caused by the downward shift of the molecular layer to the denser disk region. If we would take the disk vertical expansion due to increased heating into account, the peak of relative abundance for these components would probably reside in the region of smaller density, thus, suppressing the increase in column densities. This calls into question the ability of CO to be a tracer of dust evolution within the framework of our model. However, dust growth may affect not CO itself, but its isotopic ratios (Visser et al. 2009).

Another issue, which should be addressed properly in the future, is the possible interrelation between chemical and physical structure of the disk with evolving dust. This interrelation has already been discussed from the point of view of thermal balance in the disk (e.g., Jonkheid et al. 2007). However, dust evolution may also lead to significant changes in the fractional ionization, which is an important dynamical parameter, especially if turbulence in disks is excited due to the magnetorotational instability (Ilgner & Nelson 2008). All of this calls for more self-consistency not only between disk structure and grain evolution, but also between these two factors and chemistry.

The next step is to include time dependence in the model. Two of the three ingredients of our model (disk structure and grain ensemble properties) explicitly imply that the disk is in a steady state. The third ingredient (chemistry) is formally time-dependent, but produces steady-state abundances for most species. This is the reasonable outcome, given the equilibrium nature of the other two ingredients. Our results represent only a snapshot of the disk at an early (or even the earliest) stage of grain evolution. However, at some later stage, the grain growth timescale may become short enough to be comparable with the timescale of various chemical transformations. With the current model we cannot say what impact on chemistry possible further grain growth, beyond what the Birnstiel model can currently

calculate, would have, even though some hints are provided by model A4. In particular, we may expect higher molecular densities at the disk periphery, with the molecular layer extending down to the midplane. This confirms the earlier suggestion that observations of gas-phase CO and water molecules in a cold disk region can be explained by an increase in grain size. Further improvements in the dust growth model are also needed. This field now represents an area of active research, both theoretical and experimental, and there are certain indications that grain evolution is not limited to simply sticking and fragmenting (e.g., Zsom et al. 2010).

Another issue that may become more important with the grain ensemble containing large grains is the treatment of grain surface chemistry. Currently, in chemical modeling we consider grains of equal “effective mean size” instead of the real grain size distribution. We believe that this simplification does not dramatically affect results of this study. The average grain size defined according to (9) is close to the size of grains that dominate the total grain surface area available for surface chemistry. In other words, most of the surface chemistry occurs on grains of similar sizes. Also, Acharyya & Herbst (in preparation) constructed a chemical model with grains of several grain sizes in order to reproduce the grain size distribution. They found its results to be quite similar to those obtained with a single grain size. However, the problem may be more complicated as the temperature of an individual grain depends on its size. For smallest grains, stochastic heating becomes important, which makes it impossible to assign a single temperature to them. These questions are not trivial and worth to be considered in a separate study. In this work, we do not have grains of extremely small radii ($R \leq 10^{-6}$ cm). So, the considerations above should be of only a limited importance here.

Finally, transport processes are an important evolutionary factor in an *accretion* disk. At least, some of the differences between models GS and A5, like the enhanced depletion layer in model A5, are quite localized. One does need to account for possible gas mixing to check whether these differences can survive in a more dynamic medium. The radial motion of grains has to be included in a realistic treatment of the disk evolution.

6. Conclusions

We investigated the chemical evolution of the protoplanetary disk around a T Tauri star. The thermal and density structures of the disk are calculated with a 1+1D α -viscosity model. The processes of grain coagulation, fragmentation, and sedimentation were modeled as described in Brauer et al. (2008b) and Birnstiel et al. (2010). The initial dust ensemble is the standard MRN grain size distribution (Mathis et al. 1977). Using the final grain

size distribution (at $t = 2$ Myrs) and the 1+1D disk structure, we calculated the vertical distribution of the dust in the disk, assuming stirring-settling equilibrium according to Dullemond & Dominik (2004). For this distribution, we calculated the approximate UV field in the disk, and simulated the chemical evolution of the disk over 2 Myr. Results for three dust models were compared: (1) a classical dust model, with uniform spherical particles of $0.1\mu\text{m}$ and a gas-to-dust mass ratio of 100 (model A5); (2) a simplified grain growth model, with larger grains of $1\mu\text{m}$ (model A4); (3) a detailed grain growth model (model GS). The main results of the work can be summarized as follows:

- The fragmentation of grains due to collisions keeps a population of small dust particles in the disk, which dominate the total grain surface area crucial for chemical evolution of the disk. This effect reduces the impact of grain growth on the chemical structure of the disk. Grain growth proceeds fast in low-mass T Tauri disks at distances $\leq 20 - 50$ AU where the steady-state grain size distribution is reached in a few thousand years. Outside this radius, up to 10^6 years is needed to reach steady state at $R \geq 100$ AU. Furthermore, grain coagulation is limited there, and increases the average grain size by no more than an order of magnitude in the midplane. After 2 Myrs of evolution, the average grain size in the disk midplane varies between 10^{-4} cm at $R = 10$ AU, and $2 \cdot 10^{-5}$ cm at $R = 550$ AU. The dust-to-gas mass ratios in the same distance range are confined between $\sim 10^{-6}$ and 0.02.
- The net effect of the dust settling and growth is a reduction of the total grain surface, and higher UV irradiation rates in the upper disk. The chemical structure of an evolved disk still has three layers, but the intermediate molecular layer gets wider, and shifts closer to the midplane. Therefore, the abundances and column densities of many species are enhanced by a factor of 3 – 100, even for such a moderate grain growth.
- A simplified model of grain growth, in which the dust-to-gas mass ratio is kept constant and grain size is simply increased by one order of magnitude, is not sufficient to reproduce the chemical evolution of a disk with evolving dust. For example, the column density of H_3^+ , which is proposed to be sensitive to grain growth (Aikawa & Nomura 2006), exhibits a high sensitivity to grain growth in our simple model, but not in the model with a detailed treatment of grain growth and sedimentation.
- Grain evolution suppresses the formation of organic molecules in icy mantles, but also enhances gas-phase molecular abundances. In particular, water and CO abundances are enhanced in the cold midplane.
- We propose a few observational tracers of grain evolution process. These are the column densities of gas-phase molecules, such as C_2H , HC_{2n+1}N ($n = 0 - 3$), H_2O for the inner

disk. The abundance ratio of C_2H_2/HCN may serve as a grain evolution tracer in outer disk, as well as the abundance of CH_3OH . The composition of the ice mantles of interstellar grains seen in scattered light in the intermediate disk layer (around $\tau=1$) may also serve as a tracer of grain evolution.

7. Acknowledgements

We are grateful to Dr. Dmitry Semenov for fruitful and stimulating discussions, to Prof. Jürgen Blum for the information about collisional properties of different dust materials and to anonymous referee whose suggestions helped to improve the presentation of our results. DW's work is supported by the Federal Targeted Program "Scientific and Educational Human Resources of Innovation-Driven Russia" for 2009-2013. This research has made use of NASA's Astrophysics Data System.

REFERENCES

- Acke, B., Bouwman, J., Juhász, A., Henning, T., van den Ancker, M. E., Meeus, G., Tielens, A. G. G. M., & Waters, L. B. F. M. 2010, *ApJ*, 718, 558
- Aikawa, Y. & Nomura, H. 2006, *ApJ*, 642, 1152
- Aikawa, Y., van Zadelhoff, G. J., van Dishoeck, E. F., & Herbst, E. 2002, *A&A*, 386, 622
- Andrews, S. M. & Williams, J. P. 2007, *ApJ*, 659, 705
- Apai, D., Pascucci, I., Sterzik, M. F., van der Blik, N., Bouwman, J., Dullemond, C. P., & Henning, T. 2004, *A&A*, 426, L53
- Ayres, T. R. 2010, *ApJS*, 187, 149
- Bergin, E., Calvet, N., D'Alessio, P., & Herczeg, G. J. 2003, *ApJ*, 591, L159
- Bergin, E. A., Hogerheijde, M. R., Brinch, C., Fogel, J., Yıldız, U. A., Kristensen, L. E., van Dishoeck, E. F., Bell, T. A., Blake, G. A., Cernicharo, J., Dominik, C., Lis, D., Melnick, G., Neufeld, D., Panić, O., Pearson, J. C., Bachiller, R., Baudry, A., Benedettini, M., Benz, A. O., Bjerkerli, P., Bontemps, S., Braine, J., Bruderer, S., Caselli, P., Codella, C., Daniel, F., di Giorgio, A. M., Doty, S. D., Encrenaz, P., Fich, M., Fuente, A., Giannini, T., Goicoechea, J. R., de Graauw, T., Helmich, F., Herczeg, G. J., Herpin, F., Jacq, T., Johnstone, D., Jørgensen, J. K., Larsson, B., Liseau, R.,

- Marseille, M., Mc Coey, C., Nisini, B., Olberg, M., Parise, B., Plume, R., Risacher, C., Santiago-García, J., Saraceno, P., Shipman, R., Tafalla, M., van Kempen, T. A., Visser, R., Wampfler, S. F., Wyrowski, F., van der Tak, F., Jellema, W., Tielens, A. G. G. M., Hartogh, P., Stützki, J., & Szczerba, R. 2010, *A&A*, 521, L33+
- Bethell, T. & Bergin, E. 2009, *Science*, 326, 1675
- Birnstiel, T., Dullemond, C. P., & Brauer, F. 2009, *A&A*, 503, L5
- . 2010, *A&A*, 513, A79+
- Bourdon, E. B., Prince, R. H., & Duley, W. W. 1982, *ApJ*, 260, 909
- Bouwman, J., Henning, T., Hillenbrand, L. A., Meyer, M. R., Pascucci, I., Carpenter, J., Hines, D., Kim, J. S., Silverstone, M. D., Hollenbach, D., & Wolf, S. 2008, *ApJ*, 683, 479
- Bouwman, J., Meeus, G., de Koter, A., Hony, S., Dominik, C., & Waters, L. B. F. M. 2001, *A&A*, 375, 950
- Brauer, F., Dullemond, C. P., & Henning, T. 2008a, *A&A*, 480, 859
- . 2008b, *A&A*, 480, 859
- Ciesla, F. J. 2007, *ApJ*, 654, L159
- Cortes, S. R., Meyer, M. R., Carpenter, J. M., Pascucci, I., Schneider, G., Wong, T., & Hines, D. C. 2009, *ApJ*, 697, 1305
- D’Alessio, P., Calvet, N., Hartmann, L., Lizano, S., & Cantó, J. 1999, *ApJ*, 527, 893
- D’Alessio, P., Canto, J., Calvet, N., & Lizano, S. 1998, *ApJ*, 500, 411
- Draine, B. T. 1978, *ApJS*, 36, 595
- Draine, B. T. & Bertoldi, F. 1996, *ApJ*, 468, 269
- Draine, B. T. & Lee, H. M. 1984, *ApJ*, 285, 89
- Dullemond, C. P. & Dominik, C. 2004, *A&A*, 421, 1075
- . 2005, *A&A*, 434, 971
- Dutrey, A., Guilloteau, S., & Guelin, M. 1997, *A&A*, 317, L55

- Dutrey, A., Guilloteau, S., Piétu, V., Chapillon, E., Gueth, F., Henning, T., Launhardt, R., Pavlyuchenkov, Y., Schreyer, K., & Semenov, D. 2008, *A&A*, 490, L15
- Dutrey, A., Henning, T., Guilloteau, S., Semenov, D., Piétu, V., Schreyer, K., Bacmann, A., Launhardt, R., Pety, J., & Gueth, F. 2007, *A&A*, 464, 615
- Elias, J. H. 1978, *ApJ*, 224, 857
- Fedele, D., van den Ancker, M. E., Henning, T., Jayawardhana, R., & Oliveira, J. M. 2010, *A&A*, 510, A72+
- Garrod, R. T., Vasyunin, A. I., Semenov, D. A., Wiebe, D. S., & Henning, T. 2009, *ApJ*, 700, L43
- Geers, V. C., Augereau, J., Pontoppidan, K. M., Dullemond, C. P., Visser, R., Kessler-Silacci, J. E., Evans, II, N. J., van Dishoeck, E. F., Blake, G. A., Boogert, A. C. A., Brown, J. M., Lahuis, F., & Merín, B. 2006, *A&A*, 459, 545
- Glassgold, A. E., Najita, J., & Igea, J. 1997, *ApJ*, 480, 344
- Gorti, U. & Hollenbach, D. 2009, *ApJ*, 690, 1539
- Graham, J. R., Kalas, P. G., & Matthews, B. C. 2007, *ApJ*, 654, 595
- Güttler, C., Blum, J., Zsom, A., Ormel, C. W., & Dullemond, C. P. 2010, *A&A*, 513, A56+
- Haisch, K. E., Lada, E. A., & Lada, C. J. 2001, *ApJ*, 553, L153
- Hasegawa, T. I., Herbst, E., & Leung, C. M. 1992, *ApJS*, 82, 167
- Hayashi, C. 1981, in *IAU Symposium, Vol. 93, Fundamental Problems in the Theory of Stellar Evolution*, ed. D. Sugimoto, D. Q. Lamb, & D. N. Schramm, 113–126
- Henning, T. 2008, *Physica Scripta Volume T*, 130, 014019
- Henning, T., Semenov, D., Guilloteau, S., Dutrey, A., Hersant, F., Wakelam, V., Chapillon, E., Launhardt, R., Piétu, V., & Schreyer, K. 2010, *ApJ*, 714, 1511
- Herczeg, G. J., Linsky, J. L., Valenti, J. A., Johns-Krull, C. M., & Wood, B. E. 2002, *ApJ*, 572, 310
- Hernández, J., Hartmann, L., Calvet, N., Jeffries, R. D., Gutermuth, R., Muzerolle, J., & Stauffer, J. 2008, *ApJ*, 686, 1195
- Ilgner, M. & Nelson, R. P. 2008, *A&A*, 483, 815

- Jonkheid, B., Dullemond, C. P., Hogerheijde, M. R., & van Dishoeck, E. F. 2007, *A&A*, 463, 203
- Jonkheid, B., Faas, F. G. A., van Zadelhoff, G.-J., & van Dishoeck, E. F. 2004, *A&A*, 428, 511
- Jonkheid, B., Kamp, I., Augereau, J.-C., & van Dishoeck, E. F. 2006, *A&A*, 453, 163
- Kessler-Silacci, J., Augereau, J.-C., Dullemond, C. P., Geers, V., Lahuis, F., Evans, II, N. J., van Dishoeck, E. F., Blake, G. A., Boogert, A. C. A., Brown, J., Jørgensen, J. K., Knez, C., & Pontoppidan, K. M. 2006, *ApJ*, 639, 275
- Lee, H., Herbst, E., Pineau des Forets, G., Roueff, E., & Le Bourlot, J. 1996, *A&A*, 311, 690
- Lommen, D., Maddison, S. T., Wright, C. M., van Dishoeck, E. F., Wilner, D. J., & Bourke, T. L. 2009, *A&A*, 495, 869
- Mathis, J. S., Rumpl, W., & Nordsieck, K. H. 1977, *ApJ*, 217, 425
- Mayor, M. & Frei, P.-Y. 2003, *New Worlds in the Cosmos* (*New Worlds in the Cosmos*, by Michel Mayor and Pierre-Yves Frei and Translated by Boud Roukema, pp. 260. ISBN 0521812070. Cambridge, UK: Cambridge University Press, October 2003.)
- Mayor, M. & Queloz, D. 1995, *Nature*, 378, 355
- Nakagawa, Y., Nakazawa, K., & Hayashi, C. 1981, *Icarus*, 45, 517
- Natta, A., Testi, L., Calvet, N., Henning, T., Waters, R., & Wilner, D. 2007, in *Protostars and Planets V*, ed. B. Reipurth, D. Jewitt, & K. Keil, 767–781
- Öberg, K. I., Fuchs, G. W., Awad, Z., Fraser, H. J., Schlemmer, S., van Dishoeck, E. F., & Linnartz, H. 2007, *ApJ*, 662, L23
- Oliveira, I., Merín, B., Pontoppidan, K. M., van Dishoeck, E. F., Overzier, R. A., Hernández, J., Sicilia-Aguilar, A., Eiroa, C., & Montesinos, B. 2009, *ApJ*, 691, 672
- Ormel, C. W. & Cuzzi, J. N. 2007, *A&A*, 466, 413
- Ormel, C. W., Spaans, M., & Tielens, A. G. G. M. 2007, *A&A*, 461, 215
- Pascucci, I., Apai, D., Luhman, K., Henning, T., Bouwman, J., Meyer, M. R., Lahuis, F., & Natta, A. 2009, *ApJ*, 696, 143
- Podosek, F. A. & Cassen, P. 1994, *Meteoritics*, 29, 6

- Qi, C. 2000, PhD thesis, California Institute of Technology, Pasadena, California
- Rodmann, J., Henning, T., Chandler, C. J., Mundy, L. G., & Wilner, D. J. 2006, *A&A*, 446, 211
- Salyk, C., Blake, G. A., Boogert, A. C. A., & Brown, J. M. 2009, *ApJ*, 699, 330
- Sano, T., Miyama, S. M., Umebayashi, T., & Nakano, T. 2000, *ApJ*, 543, 486
- Schmitt, W., Henning, T., & Mucha, R. 1997, *A&A*, 325, 569
- Semenov, D., Pavlyuchenkov, Y., Henning, T., Wolf, S., & Launhardt, R. 2008, *ApJ*, 673, L195
- Semenov, D., Wiebe, D., & Henning, T. 2004, *A&A*, 417, 93
- Shakura, N. I. & Sunyaev, R. A. 1973, *A&A*, 24, 337
- Sicilia-Aguilar, A., Bouwman, J., Juhász, A., Henning, T., Roccatagliata, V., Lawson, W. A., Acke, B., Feigelson, E. D., Tielens, A. G. G. M., Decin, L., & Meeus, G. 2009, *ApJ*, 701, 1188
- Sicilia-Aguilar, A., Hartmann, L., Calvet, N., Megeath, S. T., Muzerolle, J., Allen, L., D’Alessio, P., Merín, B., Stauffer, J., Young, E., & Lada, C. 2006, *ApJ*, 638, 897
- Terada, H., Tokunaga, A. T., Kobayashi, N., Takato, N., Hayano, Y., & Takami, H. 2007, *ApJ*, 667, 303
- Testi, L., Natta, A., Shepherd, D. S., & Wilner, D. J. 2003, *A&A*, 403, 323
- Thalmann, C., Grady, C. A., Goto, M., Wisniewski, J. P., Janson, M., Henning, T., Fukagawa, M., Honda, M., Mulders, G. D., Min, M., Moro-Martín, A., McElwain, M. W., Hodapp, K. W., Carson, J., Abe, L., Brandner, W., Egner, S., Feldt, M., Fukue, T., Golota, T., Guyon, O., Hashimoto, J., Hayano, Y., Hayashi, M., Hayashi, S., Ishii, M., Kandori, R., Knapp, G. R., Kudo, T., Kusakabe, N., Kuzuhara, M., Matsuo, T., Miyama, S., Morino, J., Nishimura, T., Pyo, T., Serabyn, E., Shibai, H., Suto, H., Suzuki, R., Takami, M., Takato, N., Terada, H., Tomono, D., Turner, E. L., Watanabe, M., Yamada, T., Takami, H., Usuda, T., & Tamura, M. 2010, *ApJ*, 718, L87
- Thrane, K., Bizzarro, M., & Baker, J. A. 2006, *ApJ*, 646, L159
- Udry, S. & Santos, N. C. 2007, *ARA&A*, 45, 397

- Umebayashi, T. & Nakano, T. 1980, PASJ, 32, 405
- van Boekel, R., Min, M., Leinert, C., Waters, L. B. F. M., Richichi, A., Chesneau, O., Dominik, C., Jaffe, W., Dutrey, A., Graser, U., Henning, T., de Jong, J., Köhler, R., de Koter, A., Lopez, B., Malbet, F., Morel, S., Paresce, F., Perrin, G., Preibisch, T., Przygodda, F., Schöller, M., & Wittkowski, M. 2004, Nature, 432, 479
- van Dishoeck, E. F., Jonkheid, B., & van Hemert, M. C. 2006, Chemical Evolution of the Universe, Faraday Discussions, volume 133, 2006, p.231, 133, 231
- van Zadelhoff, G.-J., Aikawa, Y., Hogerheijde, M. R., & van Dishoeck, E. F. 2003, A&A, 397, 789
- Vasyunin, A. I., Semenov, D., Henning, T., Wakelam, V., Herbst, E., & Sobolev, A. M. 2008, ApJ, 672, 629
- Vasyunin, A. I., Semenov, D. A., Wiebe, D. S., & Henning, T. 2009, ApJ, 691, 1459
- Visser, R., van Dishoeck, E. F., & Black, J. H. 2009, A&A, 503, 323
- Wasson, J. T. & Kallemeyn, G. W. 1988, Royal Society of London Philosophical Transactions Series A, 325, 535
- Weidenschilling, S. J. 1977, Ap&SS, 51, 153
- . 1997, Icarus, 127, 290
- Weingartner, J. C. & Draine, B. T. 2001, ApJ, 548, 296
- Westley, M. S., Baragiola, R. A., Johnson, R. E., & Baratta, G. A. 1995, Nature, 373, 405
- Wilner, D. J., D’Alessio, P., Calvet, N., Claussen, M. J., & Hartmann, L. 2005, ApJ, 626, L109
- Woitke, P., Kamp, I., & Thi, W. 2009, A&A, 501, 383
- Zsom, A. & Dullemond, C. P. 2008, A&A, 489, 931
- Zsom, A., Ormel, C. W., Güttler, C., Blum, J., & Dullemond, C. P. 2010, A&A, 513, A57+

Table 1: Main disk model parameters

Inner radius	0.03 AU
Outer radius	550 AU
α	0.01
\dot{M} , M_{\odot} year ⁻¹	$2 \cdot 10^{-9}$
X-ray luminosity	10^{30} erg s ⁻¹
Cosmic ray ionization rate	$1.3 \cdot 10^{-17}$ s ⁻¹
Disk mass	$0.055 M_{\odot}$
Initial average grain size	10^{-5} cm

Table 2: Species sensitive to grain evolution. Observed column densities are compiled from Dutrey et al. (1997); Qi (2000); Aikawa et al. (2002); Dutrey et al. (2007), Bergin et al. (2010) and Henning et al. (2010).

Species	Column densities, cm ⁻²						Peak abundance		Observed	
	10 AU		100 AU		550 AU		n(X)/n(H)		column densities, cm ⁻²	
	A5	GS	A5	GS	A5	GS	A5	GS	DM Tau	LkCa15
CO	2.0(17)	1.1(18)	2.0(17)	9.4(17)	1.7(17)	2.9(17)	7.3(-05)	7.3(-05)	5.7(16)	9.0(17)
CO ₂	6.8(10)	9.5(13)	2.4(12)	8.5(14)	8.2(13)	9.8(14)	7.2(-08)	4.6(-07)	-	-
CH ₃ OH	1.1(03)	3.5(08)	1.9(08)	1.0(10)	4.6(09)	1.4(10)	1.2(-11)	1.2(-11)	-	-
H ₂ O	2.5(13)	1.1(16)	3.6(14)	7.0(15)	1.4(14)	2.0(15)	1.3(-06)	2.6(-06)	≤3.0(13)	-
H ₂ S	1.7(05)	1.3(10)	2.0(09)	1.1(11)	2.9(10)	3.6(10)	2.0(-11)	1.9(-11)	-	-
C ₂ H	6.3(10)	2.0(12)	2.6(12)	2.2(12)	6.7(12)	5.0(12)	1.4(-09)	1.5(-09)	2.8(13)	2.9(13)
C ₂ H ₂	6.2(10)	4.6(12)	4.5(12)	3.0(12)	4.4(12)	1.6(12)	4.0(-09)	1.3(-09)	-	-
CH ₃ CH ₃	3.0(09)	1.5(12)	1.8(10)	3.3(08)	1.3(07)	2.5(06)	3.6(-11)	2.3(-10)	-	-
H ₂ CS	8.0(05)	3.5(11)	2.7(11)	8.3(11)	2.7(10)	1.8(11)	2.2(-10)	5.6(-10)	-	-
HCN	2.6(12)	5.0(13)	6.9(12)	4.2(13)	9.0(12)	2.1(13)	1.8(-08)	9.1(-09)	2.1(12)	7.8(13)
HC ₃ N	6.8(08)	1.7(12)	4.1(11)	2.8(11)	1.1(12)	4.3(10)	9.1(-10)	1.1(-09)	-	-
HC ₅ N	4.9(08)	1.5(12)	2.1(11)	1.5(11)	1.8(11)	8.8(10)	5.9(-10)	6.5(-10)	-	-
HC ₇ N	4.7(06)	1.2(12)	6.1(10)	5.3(10)	9.2(10)	2.8(10)	3.9(-10)	6.0(-01)	-	-
HCNH ⁺	2.0(10)	2.7(11)	5.7(10)	1.3(11)	6.6(10)	6.8(10)	1.1(-10)	3.6(-11)	-	-
HCOOH	1.4(11)	6.3(13)	1.1(12)	1.3(13)	2.6(11)	2.1(12)	4.0(-09)	1.2(-08)	-	-
OCN	3.2(07)	4.3(09)	2.3(10)	1.5(12)	1.3(11)	4.2(12)	2.8(-10)	4.3(-09)	-	-
OCS	1.6(07)	9.3(10)	1.6(10)	1.5(10)	2.7(08)	4.5(08)	1.9(-11)	1.9(-11)	-	≤2.9(13)
NH ₃	1.7(11)	3.2(13)	1.1(13)	3.5(13)	8.5(12)	1.2(13)	1.3(-08)	9.4(-09)	-	-
HCO ⁺	1.1(11)	5.2(12)	2.6(12)	2.2(12)	2.2(12)	1.9(12)	2.0(-09)	7.0(-10)	6.5(12)	8.0(12)
OH	6.1(13)	1.9(14)	2.7(13)	1.2(14)	1.9(13)	1.5(14)	3.4(-08)	7.0(-08)	-	-

Table 3: Species insensitive to grain evolution. Observed column densities are compiled from Dutrey et al. (1997); Qi (2000) and Dutrey et al. (2007).

Species	Column densities						Peak abundance		Observed column densities, cm ⁻²	
	10 AU		100 AU		550 AU		A5	GS	DM Tau	LkCa15
	A5	GS	A5	GS	A5	GS				
CN	6.8(12)	2.9(13)	5.6(12)	9.6(12)	1.2(13)	1.7(13)	3.6(-09)	2.7(-09)	9.5-12(12)	6.3(14)
C	5.1(16)	5.9(15)	6.3(16)	7.4(16)	1.6(17)	2.1(17)	5.6(-05)	5.4(-05)	-	-
H ₃ ⁺	2.3(12)	3.7(12)	8.5(12)	1.2(13)	2.0(13)	2.5(13)	2.4(-09)	1.0(-09)	-	-
N ₂ H ⁺	3.0(09)	2.4(10)	1.7(10)	1.7(10)	1.9(10)	2.2(10)	6.1(-11)	2.4(-11)	1.1(11)	2.3(11)
HNC	1.9(12)	4.3(12)	2.5(12)	1.5(13)	5.4(12)	1.3(13)	6.3(-09)	4.7(-09)	9.1(11)	≤5.4(12)
C ⁺	2.5(16)	6.2(16)	3.3(16)	7.8(16)	5.0(16)	8.2(16)	7.3(-05)	7.3(-05)	-	-
CH ₃	2.8(11)	1.7(12)	4.7(12)	3.0(12)	2.4(13)	1.8(13)	7.0(-09)	1.7(-09)	-	-

Table 4: Ice composition in the disk at the surface $\tau = 1$. Only species with contribution of 1% or more are shown

Species	Ice fraction, %					
	10 AU		100 AU		550 AU	
	A5	GS	A5	GS	A5	GS
s-H ₂ O	99.8	97.3	57.4	91.0	70.0	88.9
s-NH ₃	-	1.0	-	-	1.0	5.0
s-C ₂ H ₂	-	-	-	-	4.6	1.0
s-C ₃ H ₂	-	-	20.9	3.3	16.5	1.5
s-C ₅ H ₂	-	-	12.0	-	2.1	-
s-C ₇ H ₂	-	-	5.0	-	-	-
s-C ₉ H ₂	-	-	1.3	-	-	-
s-CO ₂	-	-	-	2.0	-	-
s-H ₂ O ₂	-	-	-	-	-	1.5
s-HCN	-	-	-	-	3.1	1.0
s-HNO	-	-	-	1.0	-	-
s-H ₂ C ₄	-	-	1.0	-	1.0	-

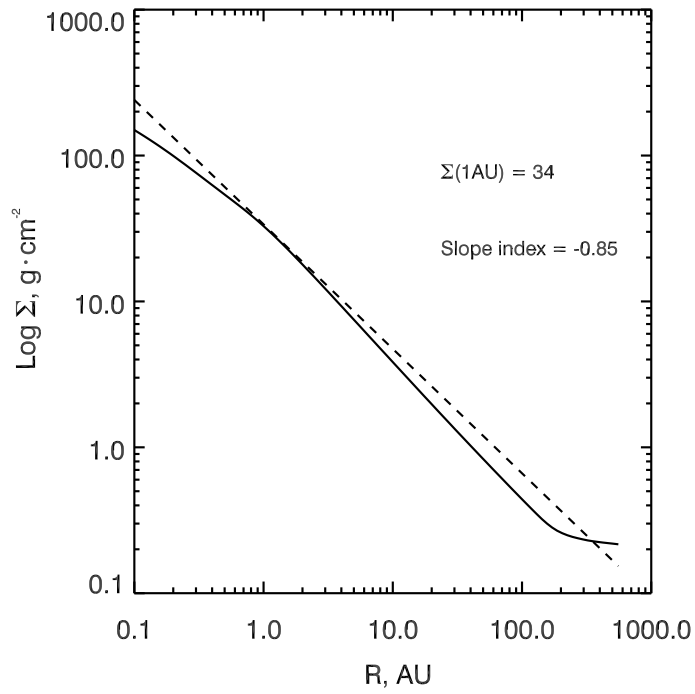


Fig. 1.— The solid line shows the radial dependence of the gas surface density in the adopted disk model. The dashed line represents a power-law fit with the slope of -0.85 .

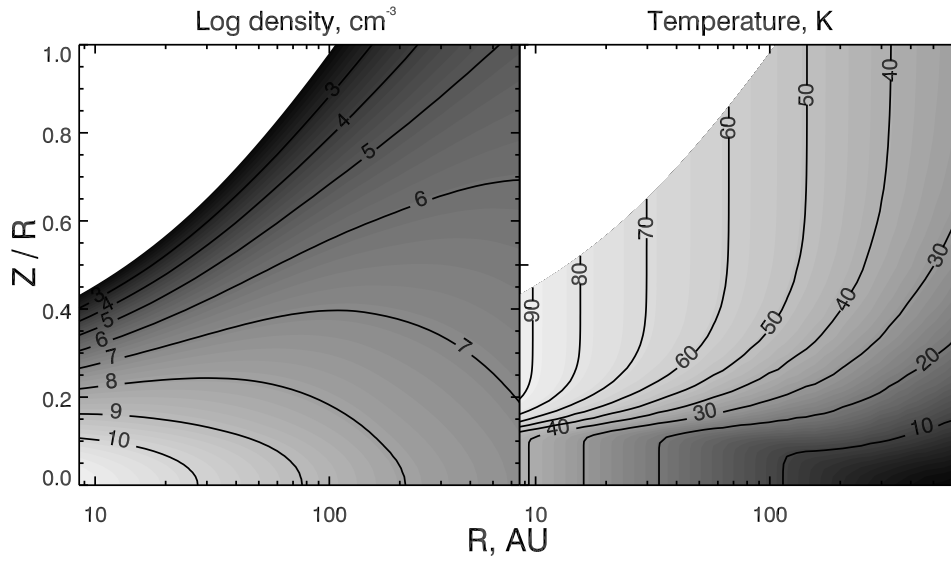


Fig. 2.— Density and temperature distribution in the adopted disk model.

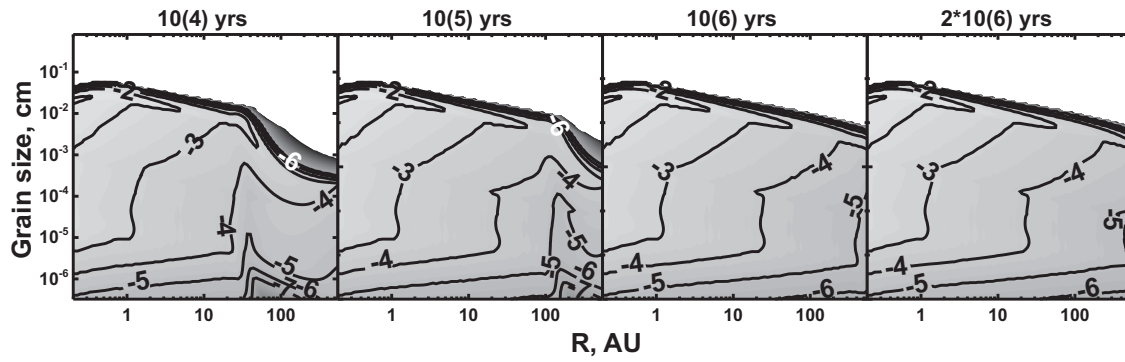


Fig. 3.— Evolution of surface density of growing dust in model GS. Contours show surface density in g cm^{-2} for dust grains of a certain size at a certain radius, so that, e.g., surface density of $0.1 \mu\text{m}$ grains at 1 AU is about $10^{-3} \text{ g cm}^{-2}$ after 10^4 years of evolution (leftmost panel). Dust growth is faster in the dense inner part of the disk. Steady-state grain size distribution is reached there between 10^4 and 10^5 years. In the outer disk, density is lower and steady-state distribution is reached between 10^6 and $2 \cdot 10^6$ years.

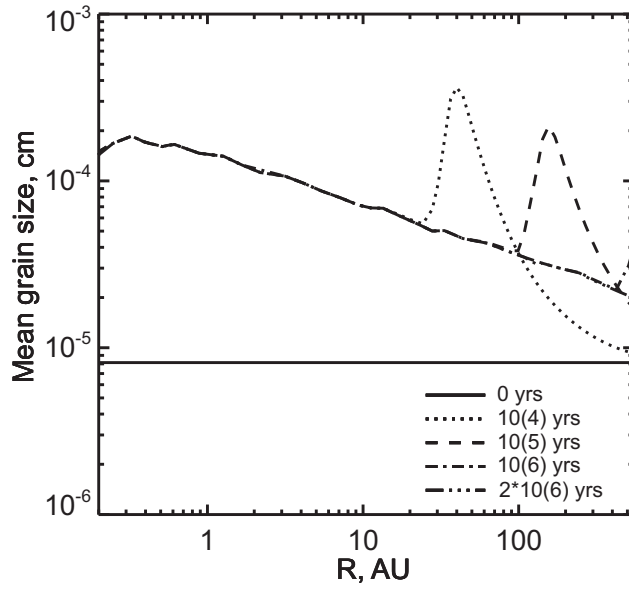


Fig. 4.— Radial distribution of the vertically-integrated average grain radius at different time moments. Averaging is performed in a way that preserves the total grain mass and surface area.

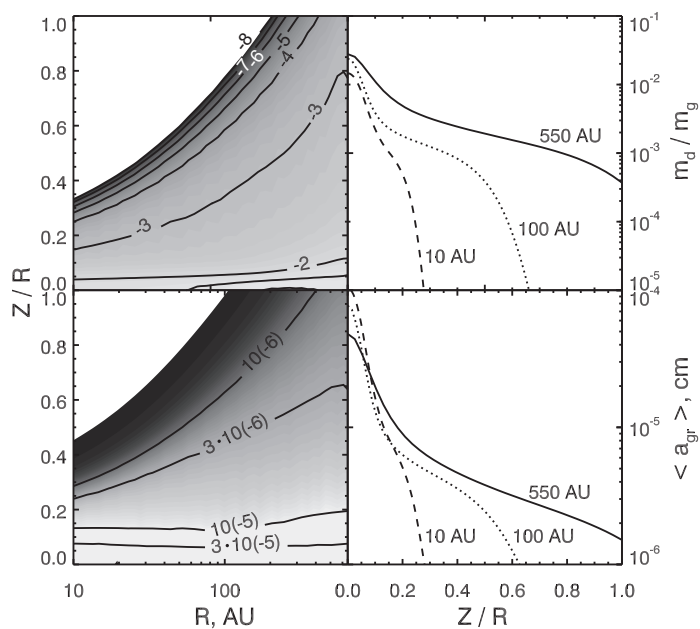


Fig. 5.— Dust-to-gas mass ratio (upper row) and an average grain radius (bottom row) in model of the disk with grain growth and sedimentation. At the left panels, 2D distributions over the disk are shown while at the right panels vertical distributions at three representative radii are plotted. Large grains that contain most of dust mass sediment to the midplane more efficiently than small ones. This reduces the dust-to-gas mass ratio above the midplane and decreases the average grain size in upper layers of the disk.

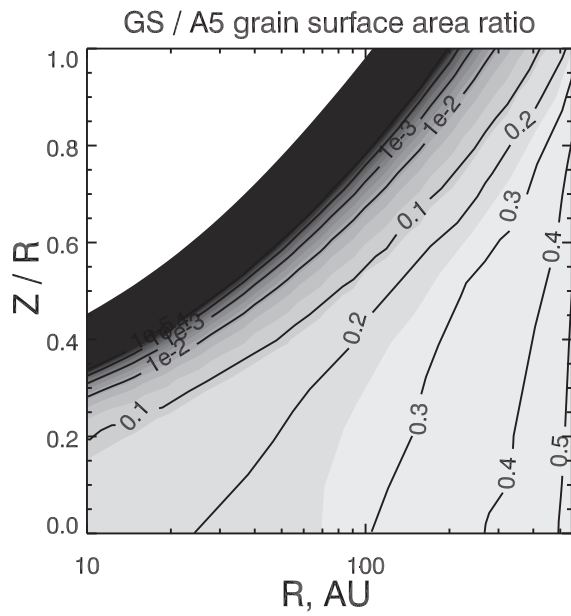


Fig. 6.— Ratio of grain surface areas in models with– and without grain evolution. Grain evolution reduces the total grain surface area. This effect is more significant in the inner disk because grain growth is more efficient there, and also above the midplane because of grain sedimentation to the midplane.

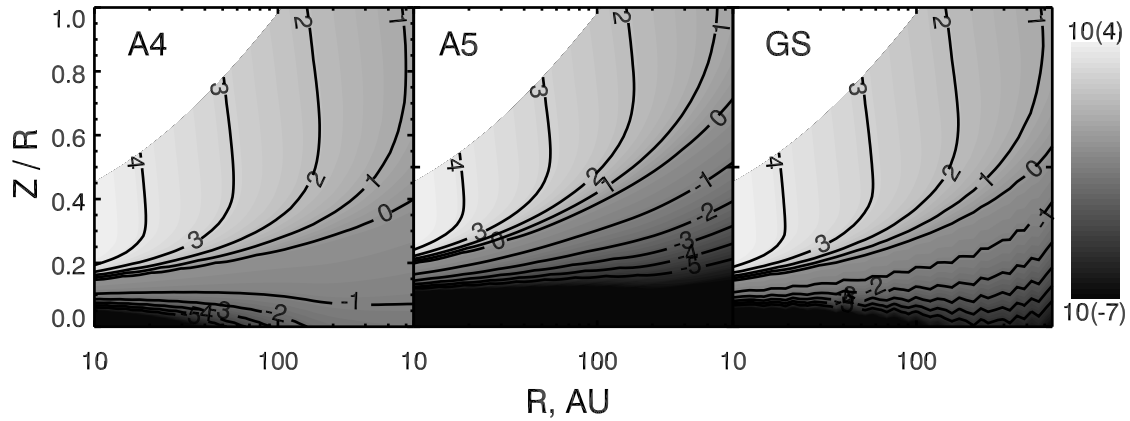


Fig. 7.— Logarithm of the UV field intensity in the disk for models A5, A4 and GS measured in units of the interstellar UV radiation field. Changes in grain properties strongly affect the amount of UV radiation penetrating into the disk. While A5 model has a dark midplane area at all radii, the model A4 disk is relatively transparent to the UV radiation beyond 100 AU. In the model GS the extent of the dark region is smaller than in model A5 (for $R \leq 100$ AU) and there is a “dim” rather than a “dark” midplane beyond 100 AU.

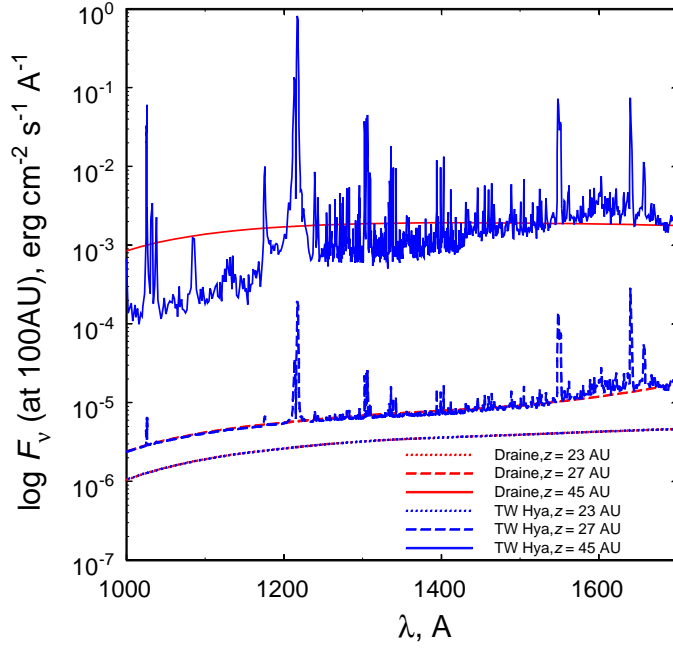


Fig. 8.— Spectrum of the UV radiation in the disk at different heights above the midplane at $R = 100$ AU in model GS. Closer to the midplane, the spectrum shape is similar to that of the ISRF because the stellar component is attenuated faster than the interstellar one. For comparison, spectrum of the scaled-up Draine field is also shown.

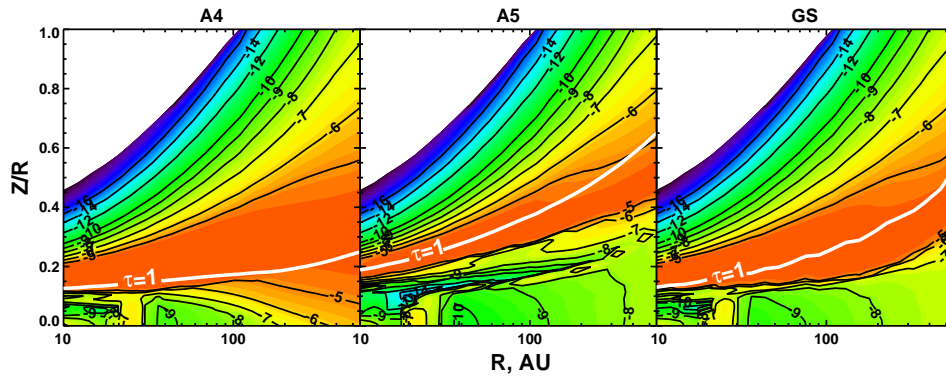


Fig. 9.— 2D distributions of CO abundance of the species relative to H₂ in models A4, A5 and GS respectively.

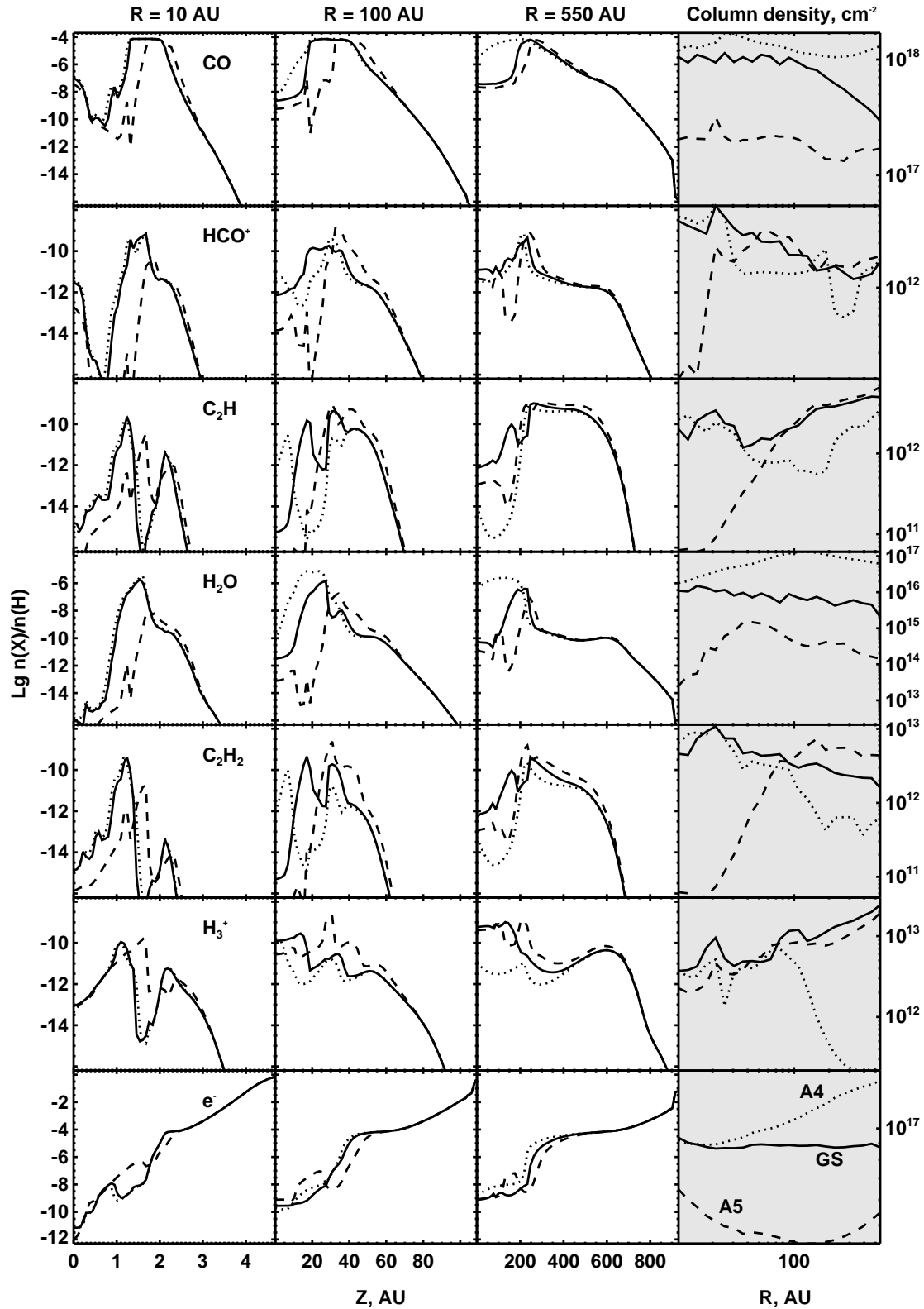


Fig. 10.— Vertical distributions at 10, 100, and 550 AU and column densities of CO, HCO⁺, C₂H, H₂O, C₂H₂, H₃⁺, and electrons in models A5 (dashed line), GS (solid line), and A4 (dotted line).

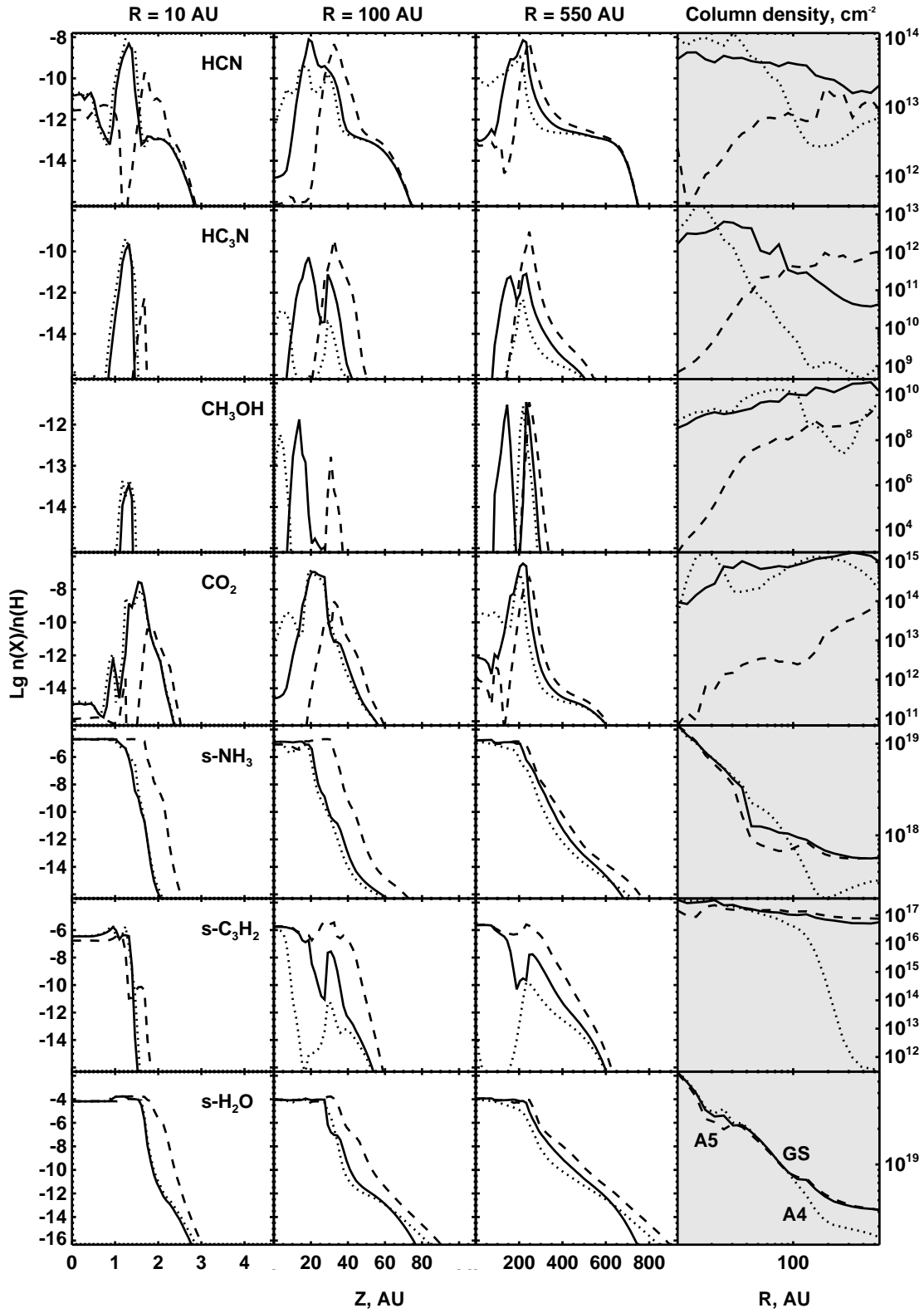


Fig. 11.— Same as in Fig. 10, but for HCN, HC₃N, CH₃OH, CO₂, s-NH₃, s-C₃H₂, s-H₂O.